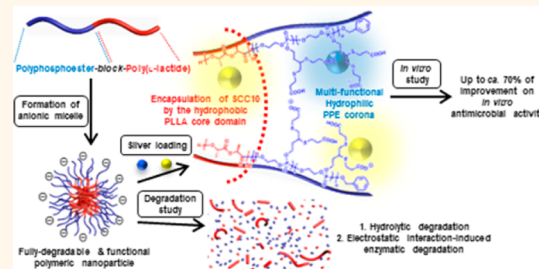


# Preparation and *in Vitro* Antimicrobial Activity of Silver-Bearing Degradable Polymeric Nanoparticles of Polyphosphoester-*block*-Poly(L-lactide)

Young H. Lim,<sup>†,‡</sup> Kristin M. Tiemann,<sup>‡,§</sup> Gyu Seong Heo,<sup>†</sup> Patrick O. Wagers,<sup>||</sup> Yohannes H. Rezenom,<sup>⊥</sup> Shiyi Zhang,<sup>†</sup> Fuwu Zhang,<sup>†</sup> Wiley J. Youngs,<sup>||</sup> David A. Hunstad,<sup>\*,‡,§</sup> and Karen L. Wooley<sup>\*,†</sup>

<sup>†</sup>Departments of Chemistry, Chemical Engineering, and Materials Science and Engineering, and Laboratory for Synthetic-Biologic Interactions, Texas A&M University, P.O. Box 30012, 3255 TAMU, College Station, Texas 77842, United States, <sup>‡</sup>Department of Pediatrics, Washington University School of Medicine, St. Louis, Missouri 63110, United States, <sup>§</sup>Department of Molecular Microbiology, Washington University School of Medicine, St. Louis, Missouri 63110, United States, <sup>||</sup>Department of Chemistry and Center for Silver Therapeutics Research, University of Akron, Akron, Ohio 44325, United States, and <sup>⊥</sup>Laboratory for Biological Mass Spectrometry, Department of Chemistry, Texas A&M University, College Station, Texas 77843, United States. <sup>\*These authors contributed equally.</sup>

**ABSTRACT** The development of well-defined polymeric nanoparticles (NPs) as delivery carriers for antimicrobials targeting human infectious diseases requires rational design of the polymer template, an efficient synthetic approach, and fundamental understanding of the developed NPs, e.g., drug loading/release, particle stability, and other characteristics. Herein, we developed and evaluated the *in vitro* antimicrobial activity of silver-bearing, fully biodegradable and functional polymeric NPs. A series of degradable polymeric nanoparticles (dNPs), composed of phosphoester and L-lactide and designed specifically for silver loading into the hydrophilic shell and/or the hydrophobic core, were prepared as potential delivery carriers for three different types of silver-based antimicrobials—silver acetate or one of two silver carbene complexes (SCCs). Silver-loading capacities of the dNPs were not influenced by the hydrophilic block chain length, loading site (*i.e.*, core or shell), or type of silver compound, but optimization of the silver feed ratio was crucial to maximize the silver loading capacity of dNPs, up to *ca.* 12% (w/w). The release kinetics of silver-bearing dNPs revealed 50% release at *ca.* 2.5–5.5 h depending on the type of silver compound. In addition, we undertook a comprehensive evaluation of the rates of hydrolytic or enzymatic degradability and performed structural characterization of the degradation products. Interestingly, packaging of the SCCs in the dNP-based delivery system improved minimum inhibitory concentrations up to 70%, compared with the SCCs alone, as measured *in vitro* against 10 contemporary epidemic strains of *Staphylococcus aureus* and eight uropathogenic strains of *Escherichia coli*. We conclude that these dNP-based delivery systems may be beneficial for direct epithelial treatment and/or prevention of ubiquitous bacterial infections, including those of the skin and urinary tract.



**KEYWORDS:** functional polymeric nanoparticles · (bio)degradable polymeric nanoparticles · nanoparticle-based antimicrobial delivery system · silver carbene complexes · *in vitro* antimicrobial efficacy · *Escherichia coli* · *Staphylococcus aureus*

**A**s slate of traditional antimicrobial agents has been employed for treatment of infectious diseases over the past decades. However, current therapeutic challenges include the rapid emergence of multidrug-resistant organisms, *e.g.*, Gram-positive pathogens, Gram-negative enteric bacteria, and *Mycobacterium tuberculosis*, and suboptimal pharmacokinetics and pharmacodynamics, *e.g.*, poor water solubility or lack of desired tissue distribution after systemic delivery.<sup>1–5</sup> Available strategies to address these barriers are limited, usually

requiring administration of more frequent or higher doses of available, traditional agents, which in turn promotes end-organ toxicities and adverse effects.<sup>6</sup> Therefore, it is imperative to identify and develop new modalities of antimicrobial treatment to circumvent these challenges; current themes include candidate antivirulence therapies that will not engender bacterial resistance, as well as targeted delivery of antimicrobials to sites of infection in order to limit systemic effects.

Silver has been used as an antimicrobial agent since ancient times, due to its broad

\* Address correspondence to wooley@chem.tamu.edu, hunstad\_d@kids.wustl.edu.

Received for review December 10, 2014 and accepted January 20, 2015.

Published online January 26, 2015  
10.1021/nn507046h

© 2015 American Chemical Society

spectrum of activity against bacterial and fungal pathogens and relatively low toxicity to human tissues. Additionally, despite its widespread topical use, e.g., in wound dressings and burn ointments, instances of bacterial resistance to the biocidal activity of silver are rare.<sup>7–12</sup> Significant efforts have been made to elucidate the antimicrobial activity of silver by employing various silver formulations, e.g., polyamidoamine dendrimer-based silver complexes and nanocomposites by Balogh *et al.*,<sup>13</sup> two-component composites of cationic polymer, poly(4-vinyl-N-hexylpyridinium bromide), and silver bromide nanoparticles by Sen *et al.*,<sup>14</sup> hybrids of silver nanoparticles with polyethylenimine-based hyperbranched polymers by Mecking *et al.*,<sup>15</sup> etc.

Given the potential of these systems, our group has been developing silver-based antimicrobial delivery from two different perspectives: (1) improving the stability of the active moiety (silver cation, Ag<sup>+</sup>), within an organometallic complex and (2) optimizing delivery of silver compounds to sites of epithelial infection by exploiting various nanoparticle templates. Youngs *et al.* designed a library of *N*-heterocyclic silver carbene complexes (SCCs), which improved the stability of Ag<sup>+</sup> to light and aqueous solution, allowed for the direct administration of silver-compounds *via* nebulization, and demonstrated the antimicrobial activity of Ag<sup>+</sup> against contemporary Gram-positive and Gram-negative pathogens.<sup>16–24</sup> In parallel, Cannon and Youngs *et al.* demonstrated sustained silver release and potent *in vitro* and *in vivo* antimicrobial efficacy of SCC10-bearing L-tyrosine polyphosphate nanoparticles (LTP NPs) against the cystic fibrosis pathogen *Pseudomonas aeruginosa*.<sup>25</sup> Meanwhile, benefiting from polymeric backbone-structured building blocks with precisely controlled architectures, surface characteristics and supramolecular assembly,<sup>26,27</sup> Cannon, Youngs, Wooley *et al.* highlighted the preparation of smaller particle size and the introduction of functionalities for attachment of targeting moieties by utilizing multifunctional shell cross-linked knedel-like polymeric nanoparticles (SCK NPs) of poly(acrylic acid)-block-polystyrene (PAA-b-PS).<sup>28,29</sup> However, in spite of promising *in vitro* data and *in vivo* therapeutic outcomes after treatment with SCK NPs bearing silver-based antimicrobials in prior studies, translational concerns remained regarding *in vivo* fate, clearance, accumulation and possible toxicity, immunogenicity and other side effects that may be elicited by the hydrocarbon backbone-based, nondegradable NPs while in mammalian hosts and persistent in the environment.<sup>30</sup>

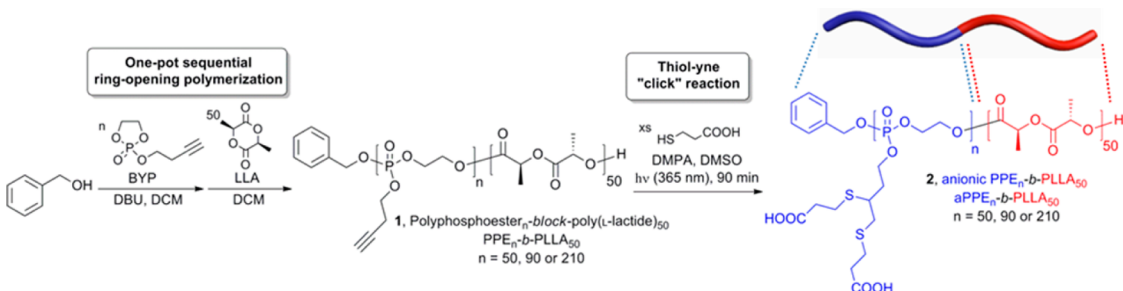
To address this limitation, we have developed biocompatible and multifunctional polymeric nanoconstructs derived from biodegradable precursors, e.g., polyphosphoesters, polycarbonates, polyesters, poly-peptides, etc. for potential application in biomedical settings.<sup>31–36</sup> We have employed a combination of state-of-the-art polymerization chemistries, “click”-type

postpolymerization chemical modification and supramolecular assembly with respect to the construction of complex and functional polymeric materials. This sequential chemical approach allows for synthetic versatility and fabrication of intricate polymeric nanoparticles for diverse pharmaceutical applications.<sup>37–43</sup> To capture this combinatorial concept, we recently demonstrated the rapid and facile synthesis of amphiphilic diblock copolymers, composed of phosphoester backbones and both carboxylate and 1,2-dithioether side chain functionalities for interactions with silver.<sup>44</sup> Micellar assemblies comprised of these block copolymers were shown to address the issues of weak silver binding and nondegradability; however, they raised alternative concerns in having phosphoric acid and ethylene glycol as two of the degradation products. Therefore, in this current work, the hydrophobic portion of the polyphosphoester backbone is replaced by poly(L-lactide), a well-known and broadly applicable polymer that is derived from the natural product lactic acid. Amphiphilic block copolymers containing phosphoester repeat units that carry carboxylate and 1,2-dithioether functionalities along the hydrophilic segment and L-lactide repeat units along the hydrophobic segment were prepared by an efficient one-pot sequential ring-opening polymerization followed by thiol-yne “click” reactions.<sup>38</sup> Subsequently, this “hybrid” polymer construct facilitated the formation of well-defined polymeric nanostructures with distinctive core–shell morphology and capable of high loading capacities for several antimicrobial silver species.

To develop potentially fully biodegradable, biocompatible polymeric NPs with the capability to deliver silver-based antimicrobials, we prepared a series of anionic dNPs from block copolymers having polyphosphoester (PPE) and poly(L-lactide) (PLLA) block segments, designed specifically for silver loading into the hydrophilic shell and/or the hydrophobic core. With the use of three different types of silver-based antimicrobials, silver acetate (AgOAc) or one of two silver carbene complexes (SCCs), comparative studies of the selection of proper dNP templates for silver-loading and release were undertaken. Then, the comprehensive degradation studies, including evaluation of hydrolytic or enzymatic degradability and identification of the degradation products, were performed for the fundamental understanding of the developed dNPs as potential delivery carriers for silver-based antimicrobials. Finally, *in vitro* antimicrobial efficacy of the selected Ag-dNPs was compared with that of inherent silver compounds against 10 contemporary epidemic strains of *Staphylococcus aureus* and eight uropathogenic strains of *Escherichia coli*.

## RESULTS AND DISCUSSION

**Rational Design of Polymer Structure and Compositions.** In designing these polymer constructs as optimized



**Scheme 1.** Synthetic route for the preparation of alkyne-functionalized diblock copolymer of phosphoester and L-lactide, PPE-*b*-PLLA, **1**, by one-pot sequential ROP, followed by post-polymerization modification via thiol-yne “click” reaction using 3-mercaptopropionic acid to prepare anionic amphiphilic diblock copolymer, aPPE-*b*-PLLA, **2**.

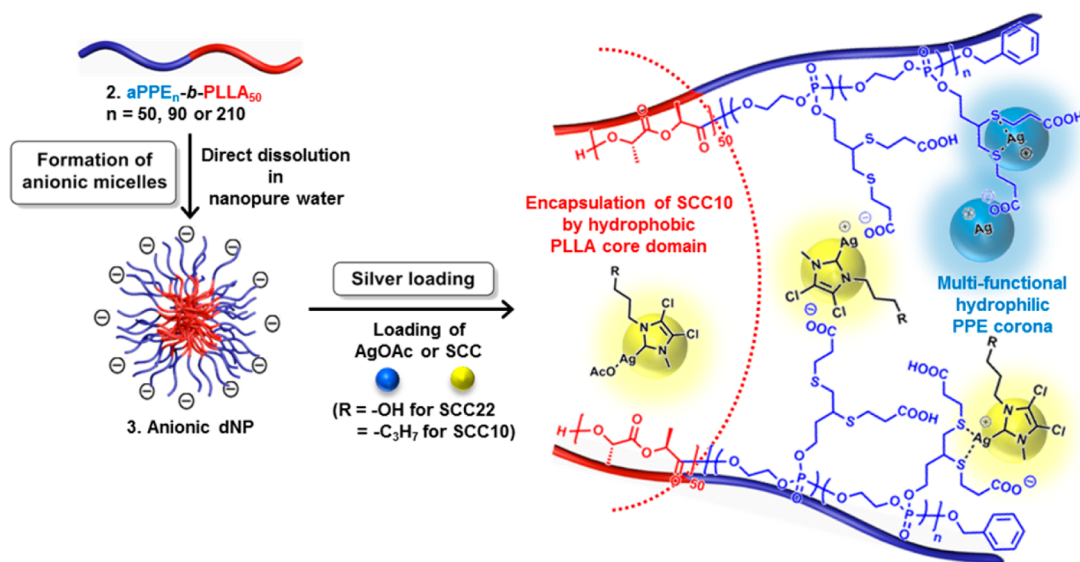
delivery carriers, several criteria were considered, *i.e.*, degradability, biocompatibility, and functionality. Its susceptibility to hydrolytic and/or enzymatic degradation and loading of hydrophobic drugs make polylactide (PLA) popular as a building block for biomedical degradable polymers.<sup>45,46</sup> However, a lack of chemical functionality and intrinsic hydrophobicity limit its use as an intelligent delivery carrier itself. To overcome this limitation, we envisioned that incorporating PPE, well-known to be biodegradable and composed of fairly hydrophilic phosphotriester linkages,<sup>31,47,48</sup> with PLA would compensate the limitations inherent to PLA alone, while also diluting the potential side effects of phosphoric acid and ethylene glycol degradation products. Furthermore, the facile introduction of pendent side functional groups on the pentavalent phosphorus atom would maximize their potential as functional delivery carriers. For instance, in this study, 1,2-dithioether and carboxylic acid side chain moieties would represent sites for silver cation loading, with the carboxylic acids also offering opportunities for conjugation with tissue-specific targeting peptides or proteins. Loading of hydrophilic and/or hydrophobic silver agents within the developed single particle template would be feasible. In addition, we postulated that nanoparticles with different hydrophilic chain lengths, *i.e.*, different dimensions of interaction sites for silver cations, may influence the silver-loading capacity of nanoparticles and, consequently, the therapeutic effects of silver-loaded nanoparticles against *in vitro* bacterial strains.

**Preparation of Functional, Degradable Polymeric Nanoparticles.** For the comparative study, each of three amphiphilic diblock copolymers with different hydrophilic PPE chain length, anionic polyphosphoester-*b*-block-poly(L-lactide) (aPPE<sub>n</sub>-b-PLLA<sub>50</sub>, *n* = 50, 90, or 210), **2**, was synthesized by one-pot sequential ring-opening polymerizations (ROP) of alkyne-functionalized cyclic phosphotriester and L-lactide followed by thiol-yne “click” reactions to introduce functionalities for interaction with Ag<sup>+</sup> and also to impart hydrophilicity to the PPE block segment (Scheme 1).<sup>38</sup> Well-defined structures of **1** were confirmed by gel permeation chromatography analysis, with monomodal molecular weight

distributions having PDI < 1.26. In addition, in all three precursor polymers, one distinct <sup>31</sup>P NMR resonance at *ca.* 0.0 ppm revealed the stability of the degradable PPE backbone during the ROPs and the workup process of **2**.

The self-assembly behaviors of the three individual polymers of aPPE<sub>n</sub>-b-PLLA<sub>50</sub>, **2** (*n* = 50, 90, or 210 for **2a**, **2b**, or **2c**, respectively), were studied by direct dissolution in nanopure water (Scheme 2). The dimensions and surface charges of the resulting dNPs, **3** (*n* = 50, 90, or 210 for **3a**, **3b**, or **3c**, respectively), were characterized by transmission electron microscopy, dynamic light scattering (DLS), atomic force microscopy (AFM) and electrophoretic light scattering, respectively. While DLS analyses of **3a** and **3b** indicated number-average hydrodynamic diameters ( $D_{h(\text{number})}$ ) of 25 and 34 nm, respectively, with monomodal size distributions (PDI < 0.13), **3c** featured the smallest  $D_{h(\text{number})}$  of 13 nm, with a broad distribution (PDI = 0.40) (Supporting Information Figure S1). The inherently hydrophilic **3c** displayed higher critical micelle concentration, *ca.* 0.5 mg/mL, owing to its long hydrophilic chain, compared with *ca.* 0.2 mg/mL of **3a** and *ca.* 0.3 mg/mL of **3b**. Meanwhile, as predicted, these three different **3** micellar formulations in aqueous solutions indicated negative surface charges, having  $\zeta$ -potential values of  $-17$  to  $-47$  mV at pH 5.0 or 7.4, as measured by electrophoretic light scattering (Supporting Information Table S1). Also, well-defined **3** assemblies were observed by TEM with comparable sizes and size distributions as observed by DLS (Supporting Information Figure S2).

In contrast to the good agreement between hydrodynamic and dry-state diameters as measured by DLS and TEM, respectively, AFM indicated significant deformation of **3** upon deposition and drying on the mica substrate (Supporting Information Figure S3). The range of *ca.* 4–9 nm in height and *ca.* 38–73 nm in diameter indicated flattening of **3**, which was anticipated based upon the presence of low  $T_g$  fluid-like shell components, *i.e.*, the PPE block segment and some degree of mixing of the shell and core components, as supported by the observation of a single  $T_g$  value for each block copolymer sample. Further



**Scheme 2.** Schematic illustration of the self-assembly of **2a**–**c** into anionic micelles, **3a**–**c**, by direct dissolution in water followed by silver loading. Schematic representation of silver cation,  $\text{Ag}^+$  (blue ball) from  $\text{AgOAc}$  and  $\text{SCC22}$  or  $\text{SCC10}$  (yellow ball) chelated into the corona or incorporated into the core of **3** (Note: the placements of the silver species within the dNP framework are proposed locations that have not been confirmed experimentally.)

quantitative analysis by AFM is complicated by the presence of substantial amounts of polymer debris and agglomerations of **3** across the substrate, which is also indicative of the fluidity of the nanoparticle assemblies.

**Preparation and Characterization of Silver-Loaded Degradable Polymeric Nanoparticles.** We intended to load three different silver-based compounds, *i.e.*, from silver acetate ( $\text{AgOAc}$ ), 1-methyl-3-(3-hydroxypropyl)-4,5-dichloroimidazol-2-ylidene silver(I) acetate ( $\text{SCC22}$ ), or 1-methyl-3-hexyl-4,5-dichloroimidazole-2-ylidene silver(I) acetate ( $\text{SCC10}$ ), into **3** by three different loading mechanisms as follows: (1) electrostatic interaction with carboxylate groups within the hydrophilic corona; (2) coordination with the two sulfur atoms of the 1,2-dithioether moieties on the side chains of the PPE block segment; and (3) encapsulation by hydrophobic interactions with the hydrophobic PLLA core of the nanoparticle (Scheme 2). Accordingly, we hypothesized that manipulation of the hydrophilic block length of **3** would influence the degree of silver-loading capacity due to the different physical dimensions of the resulting **3a**–**c** assemblies. Furthermore, it was expected that the silver-loading site, *i.e.*, shell or core, might influence the release kinetics of payloads or the antimicrobial therapeutic efficacy of silvers that are loaded *via* different loading mechanisms.

The silver-loading capacities of **3a** and **3b**, selected due to their monomodal size distributions on DLS measurement, were analyzed by inductively coupled plasma-mass spectrometry (ICP-MS) using Rh as an internal standard. Due to an ill-defined morphology, **3c** was excluded from silver loading studies. Overall, the loading capacity, measured as the weight percentage of silver loaded *vs* polymers used to form the

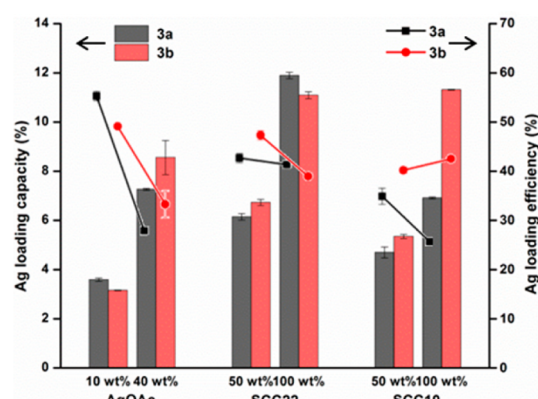


**Figure 1.** Ag-loading capacities (%) (left axis; bars) and efficiencies (%) (right axis; lines and symbols) of  $\text{AgOAc}$ -**3a**,  $\text{AgOAc}$ -**3b**,  $\text{SCC22}$ -**3a**,  $\text{SCC22}$ -**3b**,  $\text{SCC10}$ -**3a**, or  $\text{SCC10}$ -**3b** with varying silver feed (*i.e.*, 10 and 40% (w/w) of  $\text{AgOAc}$  or 50 and 100% (w/w) of  $\text{SCC22}$  and  $\text{SCC10}$ ) with respect to the mass of the polymers in the NP solutions. (Average values were calculated from triplicate experiments.).

dNPs, was dependent on the feed amount (Figure 1 and Supporting Information Table S2). For instance,  $\text{AgOAc}$ -**3b** reached *ca.* 8.6 wt % of silver loading capacity at the highest feed of  $\text{AgOAc}$  (40 wt % with respect to the mass of polymer), as compared to *ca.* 3.2 wt % at 10 wt % feed amount. Similarly, with 100 wt % feed of  $\text{SCC22}$  or  $\text{SCC10}$ , *ca.* 11 wt % loading capacities were observed for **3b**, which were about twice higher than when loaded at 50 wt % feed amount. There was no significant correlation between hydrophilic block length and silver-loading capacity with the two water-soluble silver compounds,  $\text{AgOAc}$  and  $\text{SCC22}$ . On the basis of observations of the occurrence of precipitates or no improvement of silver loading upon feeds higher

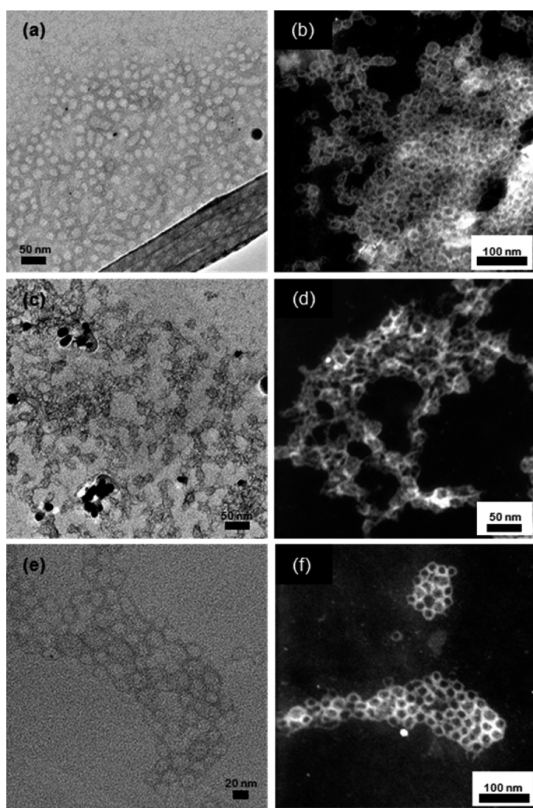


**Figure 2.** (a, c, and e) TEM bright-field and (b, d, and f) STEM dark-field images (drop deposited on carbon-coated copper grids with no stain) of (a and b) AgOAc-3b, (c and d) SCC22-3b, and (e and f) SCC10-3b.

than 40 or 100 wt % of AgOAc or SCCs, respectively, and overall insignificant difference in loading % (*ca.* < 5% in all cases) between **3a** and **3b** at 40 or 100 wt % of AgOAc or SCC22, respectively, those dNPs appeared to be already saturated with silver compounds regardless of the length of hydrophilic PPE block segment. Meanwhile, differences in the loading efficiencies, measured as the ratio of silver loaded into the dNPs to the amount of silver in the feed, between **3a** and **3b** were insignificant. Once the free silver compounds were washed away (Supporting Information Figure S4), each silver-loaded micellar nanoparticle sample was lyophilizable and redispersible in nanopure water for experimental use.

As characterized by DLS and TEM, Ag-**3a** and Ag-**3b**, each loaded by AgOAc, SCC22 or SCC10, were found to be uniform nanostructures of size and shape that agreed with the naked **3a** and **3b**, respectively, indicating that the incorporation of silver compounds did not affect the dimensions and morphology of the parent micellar assemblies (Figure 2, Supporting Information Figure S2 and Table S3). DLS analysis of Ag-**3a** and Ag-**3b** indicated  $D_{h(\text{number})}$  of *ca.* 27 and 35 nm in average, respectively, with narrow and monomodal size distributions ( $\text{PDI} < 0.26$ ). Also, size and size distributions of silver-bearing micellar nanoparticles, as observed by TEM, were comparable to those observed by DLS.

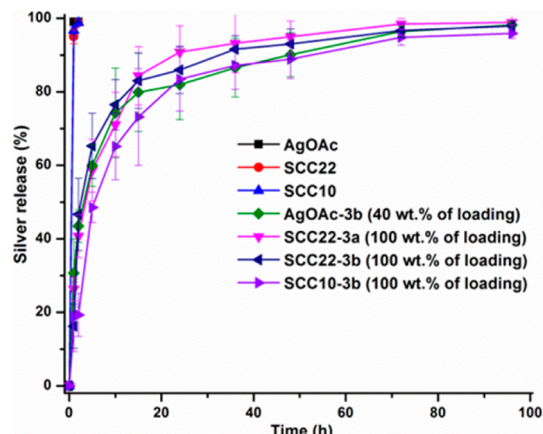
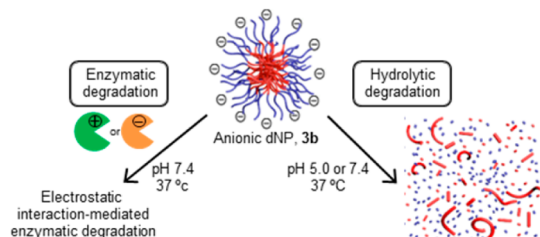


**Figure 3.** Release profiles of silver from dialysis cassettes containing solutions of silver compounds (AgOAc, SCC22 or SCC10) or silver-loaded **3a** and **3b** at 37 °C in nanopure water. (Averages were calculated from triplicate experiments.)

In addition to the quantitative analysis of silver amounts by using ICP-MS, we made an attempt to observe contrast enhancement of Ag-**3b** by using bright-field TEM and dark-field scanning transmission electron microscopy (STEM) on unstained Ag-**3b** in order to demonstrate the presence of silver within **3b** (Figure 2). The detection in the bright-field TEM images of Ag-**3b** and the dark-field STEM images of distinct illumination of silver from Ag-**3b** provided strong evidence of incorporation of silver within **3b**. It is noteworthy that these (S)TEM samples were not stained. Interestingly, hydrophobic Ag-compounds, SCC10, appeared to be located at the interface of the corona and core of **3b** in the dark-field STEM image. In each case, some elemental silver particles were detected, which may reflect reduction of  $\text{Ag}^+$  to  $\text{Ag}^0$  during the silver loading or TEM sample preparation processes. For instance, as illustrated in Figure 2 and Supporting Information Figures S5 and S6,  $\text{Ag}^0$  nanoparticles with metallic Ag lattice spacing of 2.36 nm from  $d_{\text{Ag}(111)}$  and/or 2.05 nm from  $d_{\text{Ag}(200)}$  were observed on the surface or inside the core of Ag-**3b**. Finally, the energy-dispersive X-ray spectroscopy (EDX) profile strongly confirmed the presence of silver atoms in the Ag-**3b** sample along with other abundant atoms such as phosphorus, sulfur, oxygen and carbon (Supporting Information Figure S5).

**Study of Silver-Release Kinetics.** On the basis of the silver loading results, four representative silver-loaded micellar samples showing the highest loading capacities were selected for evaluation of release kinetics. We measured [Ag] by ICP-MS in serial samples from dialysis cassettes in nanopure water at 37 °C (Figure 3 and Supporting Information Table S4). Overall, the release kinetics of all of four formulations reached a plateau with almost complete silver release by *ca.* day 3. In control studies, rapid and nearly complete (>99%) release of silver occurred for the silver compounds,



**Scheme 3.** Synthetic illustration of enzymatic (left) or hydrolytic (right) degradation of **3b**.

*i.e.*, AgOAc, SCC22 or SCC10, from dialysis cassettes in nanopure water within 1 h in the absence of dNPs, demonstrating the packaging and extended release of the silver species from the dNP constructs. Core-encapsulated SCC10 was released slightly more slowly, with time to 50% release *ca.* 5.5 h, than shell-loaded AgOAc or SCC22, *ca.* 2.5–3.5 h. Similarly, 75% release of SCC10 was achieved at *ca.* 17.5 h, slower than that of AgOAc and SCC22, *i.e.*, within *ca.* 9.5–12 h, likely due to their greater aqueous phase exposure throughout the shell and on the surface of the particle than those entrapped in the core. The fast release behavior of the present dNP-based antimicrobial system could be beneficial for direct epithelial treatment and/or prevention of ubiquitous bacterial infections, including those of the skin and urinary tract. Importantly, Ag-dNP complexes demonstrated a distinct advantage in preventing the reduction of silver, which was typically observed in aqueous solutions of the small molecule silver species within 1 day.

**Degradation Studies.** In this study, we assessed the stability of hydrolytically degradable nanoparticles in two different pH buffer solutions, 5.0 and 7.4, at 37 °C by monitoring the changes in hydrodynamic diameters ( $D_h$ ) and surface charges of **3b** by DLS and by  $\zeta$ -potential measurements, respectively (Scheme 3). The collected hydrolytic degradation products were then analyzed by using  $^{31}\text{P}$  NMR spectroscopy and structurally identified by using electrospray ionization mass spectrometry (ESI MS). Furthermore, electrostatic interaction-dependent enzymatic degradation behavior of **3b** was also investigated by using a lactate assay.

**Hydrolytic Degradation of the dNP Constructs.** The phosphoester linkage of PPEs or ester linkages of poly-lactides (PLAs) can be cleaved by spontaneous hydrolysis and/or enzymatic degradation.<sup>39,45,49–51</sup> We hypothesized that the faster hydrolysis of phosphoester linkages of PPE, compared with that of ester linkages of PLLA, would decrease the ratio of hydrophilicity/hydrophobicity, exposing hydrophobic surface patches and resulting in the precipitation of dNPs as the hydrolytic degradation proceeded (Scheme 3). Thus, aqueous buffer solutions of **3b** at pH 5.0 or 7.4 were incubated at 37 °C, and degradation profiles were assessed by measuring changes in  $D_h$  by DLS for up to 30 days (Figure 4). As shown in Figure 4,

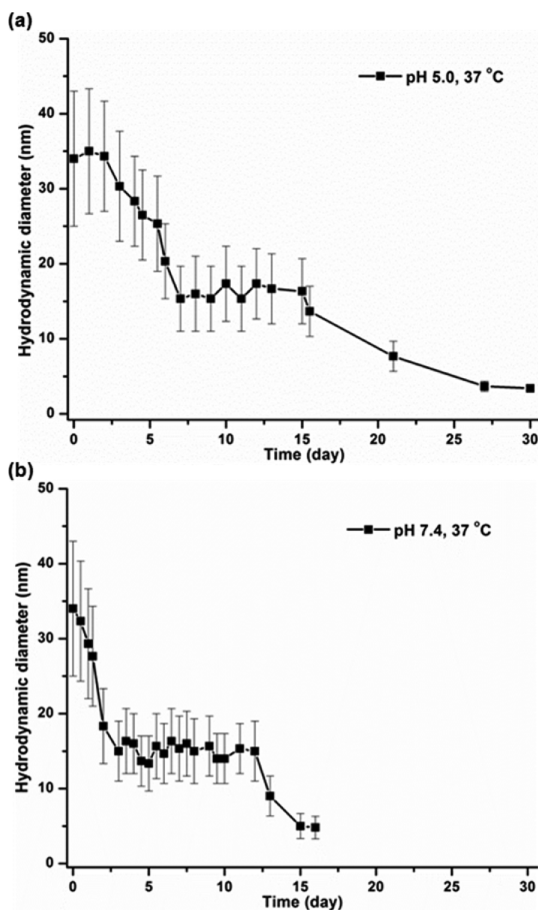


**Figure 4.** Study of dNP stability by using DLS. Changes in the hydrodynamic diameter (nm) of nanoparticles, **3b**, at pH 5.0 (a) or pH 7.4 (b) at 37 °C over time. The average values from 10 measurements, with the standard deviations calculated as the breadth of the distributions, are shown.

there was an apparent decrease in  $D_h$  with time, which might be due to hydrolytic degradation of portions of the PPE shell chains. However, the degradation was complicated by macroscopic precipitation events. Overall, the dNP assemblies in pH 5.0 and 7.4 aqueous solutions became unstable within about 2 weeks at 37 °C. In accordance with our prediction, the dNP solutions began to form visible precipitates gradually as time proceeded. After 2 weeks of incubation, a low intensity of scattered light prevented dNP detection, as measured by DLS. Meanwhile, there was no significant change in the  $\zeta$ -potential values of **3b** at pH 5.0 or pH 7.4 over this time period (Supporting Information Figure S7). Finally, in agreement with our hypothesis of backbone hydrolysis of the PPE block segment, there was a distinct shift in the  $^{31}\text{P}$  resonance frequency from –0.02 ppm for intact **3b** to 1.01 ppm for its degradation products, *i.e.*, phosphoric acid (Supporting Information Figure S8).

**Identification of the Degradation Products of **3b** by ESI Mass Spectrometry.** Previously, we reported identification of the hydrolytic degradation products of nanoparticles of poly(ethylene glycol)-block-polyphosphoester,

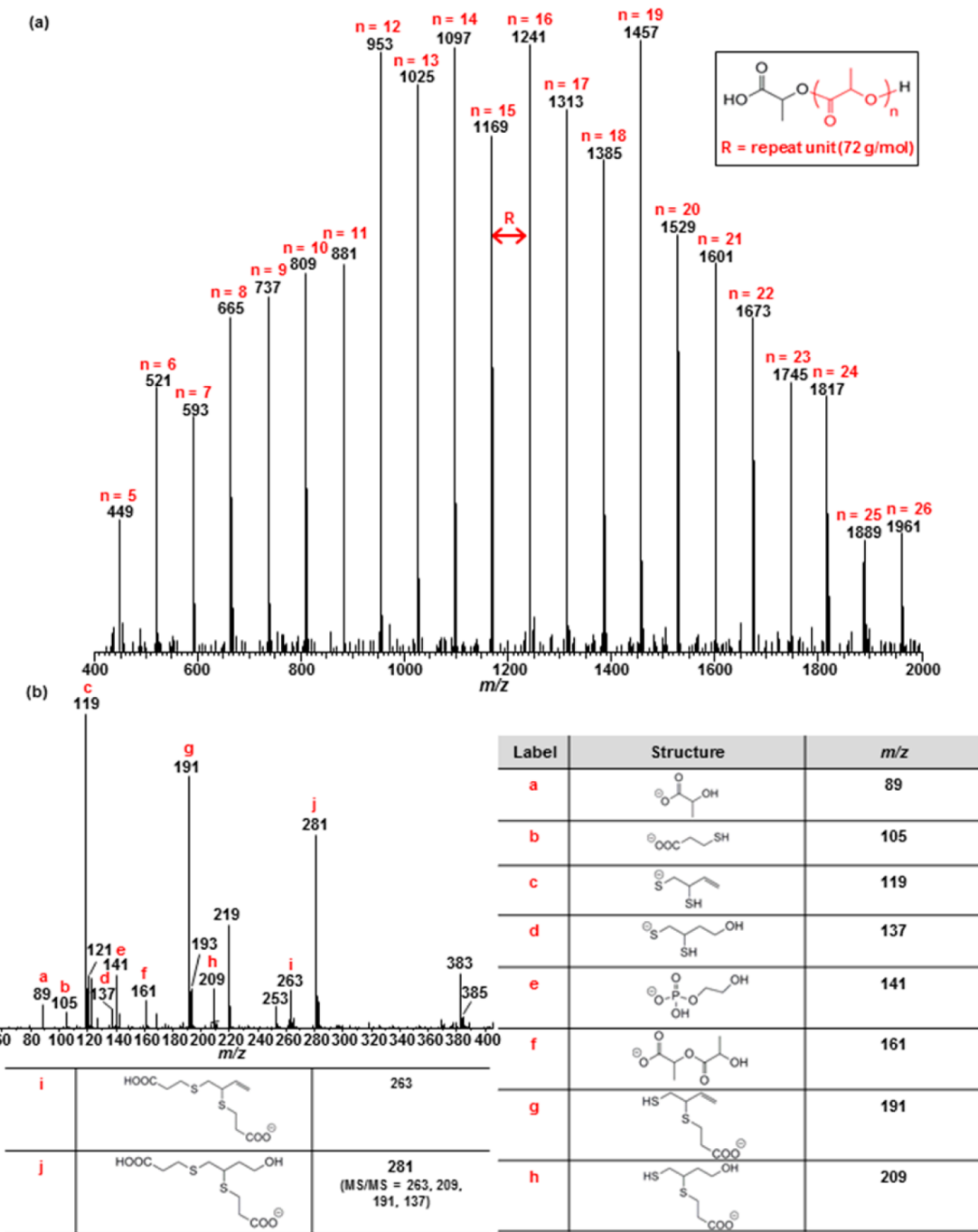


Figure 5. ESI MS analysis of the degradation products of nanoparticles, 3b. Mass spectra in negative ion mode;  $m/z$  range of 400–2000 (a) and 50–400 (b). See Supporting Information Figure S9 for the MS/MS spectrum of j.

a partially degradable diblock copolymer, by ESI MS.<sup>39</sup> In the present study, we identified the degradation products from our fully degradable diblock copolymer system **3b** by employing the same analytical approach. Solutions of **3b** in D<sub>2</sub>O were incubated at 37 °C for 35 days, at which time they were not detectable by DLS and the <sup>31</sup>P resonance signal from the intact PPE backbone had disappeared in <sup>31</sup>P NMR spectra. Given our hydrolytic degradation data, we postulated that the PPE block segment primarily becomes hydrolyzed into small molecules, *i.e.*, variants of phosphoric acids along with

side-chain moieties, while the more rigid ester backbone-based PLLA block segment would be converted into a mixture of oligomers and partially fragmented polymers of lactide. Indeed, in the  $m/z$  region below 400, the presence of derivatives of phosphoric acids (**e** in Figure 5) and side chain moieties (**j** in Figure 5) was confirmed by ESI MS, supporting our model of hydrolytic degradability of phosphotriester linkages of PPE. A number of unexpected molecular derivatives, generated by fragmentation during ESI MS measurements, were also identified by using tandem mass

spectrometry (Supporting Information Figure S9). Of note, ethylene glycol was not demonstrable as one of the degradation products, as it is not ionized in the electrospray instrument. In addition to the presence of the unimer and dimer of lactic acid (**a** and **f** in Figure 5, respectively) in the *m/z* region below 400, a series of fragments of PLLA block segments were detected, *i.e.*, oligomers and polymers with repeat units up to 26, with monomodal distribution of *m/z* at intervals of 72 Da, corresponding to a single PLLA repeat unit. No molecules were detected above *m/z* 2000 by ESI or by matrix-assisted laser desorption/ionization time-of-flight (MALDI-TOF) mass spectrometry.

**Electrostatic Interaction-Induced Enzymatic Degradation of dNP Constructs.** Our group recently reported the programmed hydrolysis of polylactide-containing nanoassemblies by electrostatic interaction-mediated enzymatic degradation behavior.<sup>52</sup> As the present constructs feature similar chemical composition, *i.e.*, a PLLA block segment, and physical properties, *i.e.*, anionic surface charge, we measured the electrostatic interaction-dependent enzymatic degradation rates of **3b** upon the addition of two model enzymes possessing positive and negative charges at physiological pH, *i.e.*, proteinase K (PK) with an isoelectric point (pl) *ca.* 8.9 and porcine liver esterase (PLE) with pl *ca.* 4.8, which can catalyze hydrolysis of poly(lactic acid). Consistent with our prior observations, treatment with PK yielded *ca.* 40% release of lactic acid, compared with *ca.* 4% release by porcine liver esterase (Supporting Information Figure S10). The accelerated production of lactic acid, reflecting degradation of the PLLA block segments, was attributed to attractive electrostatic interactions between oppositely charged **3b** and PK. In contrast, the limited enzymatic activity of PLE toward **3b** was likely due to the repulsive electrostatic interaction between the two similarly charged objects, and also due to the lower activity of PLE vs PK.

**In Vitro Antimicrobial Activity of Ag-dNPs.** It is well-known that a polymeric nanoparticle matrix may enhance the therapeutic efficacy of active agents by improving drug delivery features such as solubility, encapsulation, etc.<sup>26</sup> Thus, we evaluated the *in vitro* antimicrobial activities of silver compounds and silver-loaded micelles (**3a** or **3b**) by determining the minimal inhibitory concentrations (MICs) in Mueller-Hinton (MH) broth against eight uropathogenic strains of *E. coli* and 10 contemporary strains of *S. aureus*. Silver compounds alone and silver-loaded **3** were tested in duplicate or triplicate wells of a 96-well plate and repeated on 3–6 separate days. When loading **3b** with each of the three silver species, AgOAc at 40 wt % loading, SCC22 at 100 wt % loading and SCC10 at 100 wt % loading, comparisons were expected to be made as to the nature of the silver components with a common polymer micelle nanoparticle, each at their highest loading levels. In addition, a fourth sample, having SCC22 loaded at

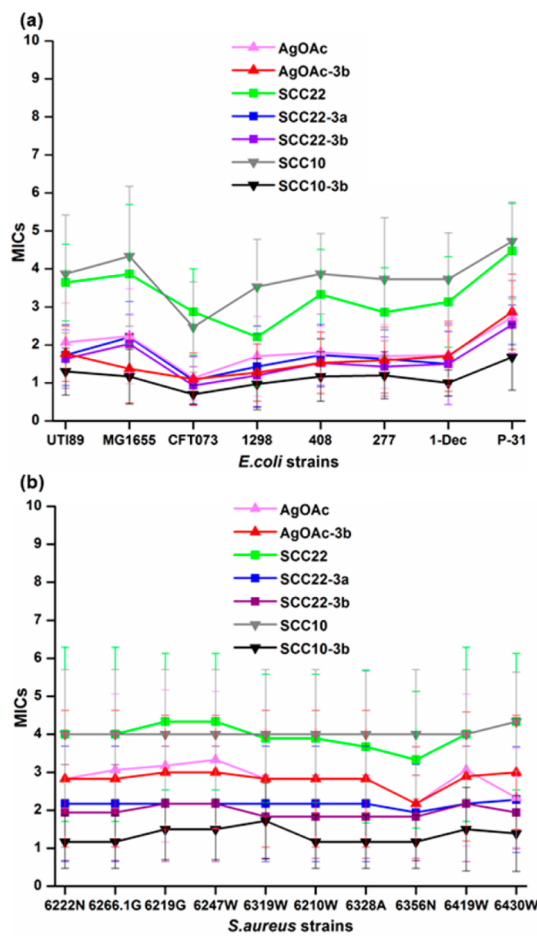


**Figure 6.** Minimum inhibitory concentration (MIC,  $\mu\text{g}/\text{mL}$  Ag) profiles of silver-compounds (AgOAc, SCC22 and SCC10) and silver-bearing micellar nanoparticles (AgOAc-3b, SCC22-3a, SCC22-3b and SCC10-3b) against (a) eight uropathogenic strains of *E. coli* and (b) 10 contemporary epidemic strains of *S. aureus*.

100 wt % into micelle **3a**, allowed for comparisons of the polymer nanoparticle with the same silver species. Aggregate results of multiple experiments comprised 9–15 trials of each sample with each bacterial strain. Overall, the MICs (expressed and compared as  $\mu\text{g}/\text{mL}$  Ag) of the silver compounds and silver-loaded nanoparticle constructs for *S. aureus* were higher than those for *E. coli* but remained physiologically relevant (1–5  $\mu\text{g}/\text{mL}$ ) (Figure 6, Tables 1 and 2, and Supporting Information Table S5). Among the three silver compounds alone, AgOAc displayed the most potent antimicrobial activity against both bacterial species; the average MIC values of AgOAc were 1.89  $\mu\text{g}/\text{mL}$  for *E. coli* and 2.84  $\mu\text{g}/\text{mL}$  for *S. aureus*, compared with 3.3 and 3.98  $\mu\text{g}/\text{mL}$  of SCC22 and 3.78 and 4.03  $\mu\text{g}/\text{mL}$  of SCC10, respectively (*p*-value of AgOAc < 0.00001 relative to that of SCC22 or SCC10 for both *E. coli* and *S. aureus*; Supporting Information Table S5). Interestingly, we observed significant improvement of antimicrobial activity of the SCJs upon nanoparticle packaging, *i.e.*, *ca.* 50 and 70% lower MICs for SCC22-**3** and SCC10-**3** vs SCC22 and SCC10, respectively (*p*-values for mean MIC

**TABLE 1. Average MICs ( $\mu\text{g/mL}$  Ag) and % Improvements of Silver Compounds (AgOAc, SCC22 and SCC10) and Silver-Bearing Micellar Nanoparticles (AgOAc-3b, SCC22-3a, SCC22-3b, and SCC10-3b) against Eight Uropathogenic Strains of *E. coli***

	AgOAc	SCC22	SCC10	
Avg. MIC	1.89	3.3	3.78	
	AgOAc-3b	SCC22-3a	SCC22-3b	SCC10-3b
Avg. MIC	1.65	1.73	1.6	1.15
% Improvement	13%	48%	52%	70%

**TABLE 2. Average MICs ( $\mu\text{g/mL}$  Ag) and % MIC Improvement for Silver Compounds (AgOAc, SCC22 and SCC10) and Silver-Bearing Micellar Nanoparticles (AgOAc-3b, SCC22-3a, SCC22-3b, and SCC10-3b) against 10 Contemporary Epidemic Strains of *S. aureus***

	AgOAc	SCC22	SCC10	
Avg. MIC	2.84	3.98	4.03	
	AgOAc-3b	SCC22-3a	SCC22-3b	SCC10-3b
Avg. MIC	2.82	2.16	1.97	1.34
% Improvement	1%	46%	51%	67%

of SCC22-3a, SCC22-3b or SCC10-3b  $< 0.00001$  relative to those of SCC22 or SCC10 for both *E. coli* and *S. aureus*). However, similar improvement was not observed when packaging AgOAc into **3b**. Although we do not yet fully understand the mechanism, Ag<sup>+</sup> in a carbene complex appeared to be more efficacious with the micellar carrier system than was Ag<sup>+</sup> in a salt format. We previously reported a similar phenomenon.<sup>29</sup> We speculate that the nanoparticle-mediated delivery system provided protection to the SCC complexes and may have facilitated delivery of the silver species locally through nonspecific association of the nanoparticles with the bacterial cells. Of note, naked **3**, with no silver loading and applied at equivalent polymer concentrations, did not display antimicrobial activity nor toxicity to cultured mammalian cells. Taken together, these Ag-dNPs exhibited antimicrobial

activities superior to small silver compounds, which supports the potential of using the developed degradable nanoparticles as an antimicrobial delivery system.

## CONCLUSIONS

In conclusion, fully degradable and functional polymeric nanoparticles as delivery carriers for silver-based antimicrobials were developed, and their *in vitro* antimicrobial efficacy and degradability were investigated. A series of nanoparticles, composed of amphiphilic diblock copolymers of phosphoester and L-lactide with varying hydrophilic chain lengths, were designed and prepared as potential delivery carriers for three different types of silver-based antimicrobials. While there was no evidence of an influence of hydrophilic chain length or loading site on the silver-loading capacity of dNPs, optimization of the feed ratio was critical to maximizing the silver loading capacity. The fast release kinetics of Ag-dNPs, typically found in the use of micelles, could be beneficial for treatment of infectious diseases, e.g., lung infections via pulmonary inhalation administration or urinary tract infections via direct inoculation of therapeutics. The dNP-based antimicrobial delivery system exhibited significant improvement in *in vitro* antimicrobial activity over the parent silver compounds, particularly with reference to the silver carbene cargo. Finally, the degradability of these NPs was demonstrated in comprehensive degradation studies, including the stability of dNPs by DLS measurement, identification of the degradation products by ESI MS, and electrostatic interaction-mediated enzymatic degradation of dNPs by lactate assays. Further studies will develop a better understanding of the fundamental interactions between bacterial cells, the dNPs and their degradation products. Moreover, conjugation of the dNPs with tissue-specific targeting proteins or peptides and determination of *in vivo* biodistribution, toxicity, and therapeutic efficacy of the Ag-dNPs against bacterial infectious diseases represent important future goals in demonstrating the translational potential of these novel nanoconstructs.

## METHODS

**Materials.** Ammonium acetate, benzoic acid, 3-butyn-1-ol, dimethyl sulfoxide (DMSO), 2,2-dimethoxy-2-phenylacetophenone, 3-mercaptopropionic acid, 3-(*N*-morpholino)propanesulfonic acid (MOPS), porcine liver esterase (PLE) (activity = 154 U mg<sup>-1</sup>, concentration = 35.6 mg of protein mL<sup>-1</sup>), proteinase K (PK) (activity = 1362 U mL<sup>-1</sup>, concentration = 36 mg of protein mL<sup>-1</sup>), silver acetate (AgOAc) and triethylamine (TEA) were used as received from Sigma-Aldrich Company. 2-Chloro-2-oxo-1,3,2-dioxaphospholane (COP, 95%) was used as received from Thermo Fisher Scientific, Inc. L-Lactide (LLA) (98%, Alfa Aesar) was purified and dried by azeotropic distillation in toluene three times. Benzyl alcohol and 1,8-diazabicyclo[5.4.0]undec-7-ene (DBU) were purchased from Sigma-Aldrich Company, and they were distilled from calcium hydride. The

dried benzyl alcohol, DBU and LLA were stored in an argon-filled glovebox until use. Tetrahydrofuran (THF) and dichloromethane (DCM) were dried through columns (J. C. Meyer Solvent Systems, Inc.). 1-Methyl-3-(3-hydroxypropyl)-4,5-dichloroimidazol-2-ylidene silver(I) acetate (silver carbene complex 22, SCC22) and 1-methyl-3-hexyl-4,5-dichloroimidazole-2-ylidene silver(I) acetate (silver carbene complex 10, SCC10) were synthesized as previously reported.<sup>53,54</sup> Spectra/Pro membranes (MWCO 12–14 kDa, Spectrum Medical Industries, Inc., Laguna Hills, CA) were used for dialysis. The cell culture 96-well flat bottom plates were purchased from Corning Costar Co. Amicon ultra centrifugal filter devices (100 kDa MWCO) were purchased from Millipore Corp (Bedford, MA). Nanopure water (18 MΩ · cm) was acquired by means of a Milli-Q water filtration system (Millipore Corp., Bedford, MA). The lactate colorimetric assay kit (ab65331)

was purchased from Abcam. Dialysis cassettes (Slide-A-Lyzer, 10 kDa MWCO) were purchased from Pierce Biotechnology, Rockford, IL.

**Instrumentation.**  $^1\text{H}$ ,  $^{13}\text{C}$ , and  $^{31}\text{P}$  NMR spectra were recorded on Inova 300 MHz spectrometers interfaced to UNIX computers using VnmrJ software. Chemical shifts were referenced to solvent resonance signals. For  $^{31}\text{P}$  NMR spectroscopy, phosphoric acid (85 wt % in  $\text{H}_2\text{O}$ ) at 0 ppm was used as an external standard. IR spectra were recorded on an IR Prestige 21 system (Shimadzu Corp., Japan) and analyzed using the IRsolution software.

Size exclusion chromatography (SEC) measurements were performed on a Waters Chromatography, Inc. (Milford, MA) system equipped with an isocratic pump model 1515, a differential refractometer model 2414, and a four-column set of 5  $\mu\text{m}$  Guard ( $50 \times 7.5$  mm), Styragel HR 4.5  $\mu\text{m}$  DMF ( $300 \times 7.5$  mm), Styragel HR 4E 5  $\mu\text{m}$  DMF ( $300 \times 7.5$  mm) and Styragel HR 2.5  $\mu\text{m}$  DMF ( $300 \times 7.5$  mm). Polymer solutions were prepared at a concentration of about 3–5 mg/mL and an injection volume of 200  $\mu\text{L}$  was used. Data collection and analysis were performed with Empower 2 v. 6.10.01.00 software (Waters, Inc.). The system was equilibrated at 70 °C in prefILTERed DMF containing 0.05 M of LiBr, which served as polymer solvent and eluent (flow rate set to 1.00 mL/min). The system was calibrated with polystyrene standards (Polymer Laboratories, Amherst, MA) ranging from 615 to 442 800 Da.

Glass transition temperatures were measured by differential scanning calorimetry (DSC) on a Mettler-Toledo DSC822 (Mettler-Toledo, Inc., Columbus, OH), with a heating rate of 10 °C/min. Measurements were analyzed by using Mettler-Toledo Star<sup>e</sup> v. 7.01 software. The  $T_g$  was taken as the midpoint of the inflection tangent, upon the third heating scan. Thermo-gravimetric analysis (TGA) was performed under  $\text{N}_2$  atmosphere using a Mettler-Toledo model TGA/SDTA851e, with a heating rate of 10 °C/min and cooling rate of 10 °C/min. Measurements were analyzed by using Mettler-Toledo Star<sup>e</sup> v. 7.01 software.

Dynamic light scattering (DLS) measurements were conducted using Delsa Nano C (Beckman Coulter, Inc., Fullerton, CA) equipped with a laser diode operating at 658 nm. Size measurements were made in nanopure water ( $n = 1.3329$ ,  $\eta = 0.890$  cP at  $25 \pm 1$  °C). Scattered light was detected at 165° angle and analyzed using a log correlator over 70 accumulations for a 3.0 mL sample in a glass sizing cell (4.0 mL capacity). The samples in the glass sizing cell were equilibrated for 30 min before measurements were made. The photomultiplier aperture and the attenuator were automatically adjusted to obtain a photon counting rate of *ca.* 10 kcps. Calculation of the particle size distribution and distribution averages was performed using CONTIN particle size distribution analysis routines. The peak averages of histograms from number distributions out of 70 accumulations were reported as the average diameters of the particles.

The  $\zeta$ -potential values of the nanoparticles were determined by Delsa Nano C particle analyzer (Beckman Coulter, Fullerton, CA) equipped with a 30 mW dual laser diode (658 nm). The  $\zeta$ -potential values of the particles in suspension were obtained by measuring the electrophoretic movement of charged particles under an applied electric field. Scattered light was detected at a 30° angle at 25 °C. The  $\zeta$ -potential was measured at five regions in the flow cell and a weighted mean was calculated. These five measurements were used to correct for electroosmotic flow that was induced in the cell due to the surface charge of the cell wall. All determinations were repeated three times.

Transmission electron microscopy (TEM) images were collected on a JEOL 1200EX, operating at 100 kV or a FEI Tecnai G2 F20 FE-TEM, operating at a voltage of 200 kV. High-resolution scanning transmission electron (STEM) microscopy was conducted on a FEI Tecnai G2 F20 FE-TEM coupled with energy-dispersive X-ray (EDX), operating at a voltage of 200 kV. The samples, as aqueous solution (5  $\mu\text{L}$ , polymer concentration at 0.25–3.75 mg/mL), were deposited onto carbon-coated copper grids. After 1 min of deposition, the excess sample was quickly wicked off using filter paper, and the grids were allowed to dry in the air for 10 min. Then, the grids were negatively stained with 5  $\mu\text{L}$  of a 2% aqueous solution of uranyl acetate. The excess

stain was wicked off using filter paper after 20 s. The sample grids were dried under vacuum at room temperature overnight before analysis.

Atomic force microscopy (AFM) was performed using a Multimode 8 system (Bruker) with an SA Fluid+ silicon probe (k 0.7 N/150 kHz, Bruker). For AFM preparation, nanoparticles were dissolved in nanopure water at 0.1 mg/mL, and 20  $\mu\text{L}$  of the sample was spin coated onto a glass coverslip. All AFM samples were stored at room temperature in a vacuum desiccator until use. AFM images were assessed with Nanoscope Analysis (Bruker).

Electrospray ionization (ESI) in negative ion mode was carried on a quadrupole ion trap mass spectrometer (LCQ-DECA, ThermoFinnigan, San Jose, CA). The sample was directly infused at 6  $\mu\text{L}/\text{min}$  of flow rate. The spray voltage was set at –4.5 kV. Sheath gas and auxiliary gas flow rates were 50 and 10 arbitrary units, respectively. Transfer capillary temperature was held at 250 °C. MS/MS experiments were performed on the same instrument at a relative collision energy of 30–32%. Xcalibur 2.0 software package (ThermoFinnigan) was used for data acquisition and processing.

Matrix-assisted laser desorption ionization (MALDI) experiments were performed on a Voyager DE-STR mass spectrometer (Applied Biosystems, Foster City, CA) under optimized conditions in positive linear mode. Ions were generated by a pulsed nitrogen laser at 337 nm and accelerated through 25 kV and 100 laser shots were used per spectrum. *trans*-2-[3-(4-t-Butylphenyl)-2-methyl-2-propenylidene]malononitrile (DCTB) and potassium trifluoroacetate (KTFA) were used as a matrix and cationization reagent, respectively. The sample, KTFA, and matrix were prepared at concentration of 1, 10, and 20 mg/mL, respectively. The sample solution was mixed with the matrix and KTFA at a volume ratio of 1:5:1. About 0.5  $\mu\text{L}$  of this mixture was deposited on a stainless steel sample holder. After being allowed to air-dry, the sample was analyzed using MALDI-TOF MS.

Ultraviolet-visible spectroscopy (UV-vis) absorption measurements were made using a UV-2550 system (Shimadzu Corp.). Measurements were performed in nanopure water in quartz cuvettes with path lengths of 1 cm.

Critical micelle concentration (CMC) values were determined by pyrene fluorescence measurements that were conducted on a RF-5301PC spectrofluorophotometer system (Shimadzu Corp., Kyoto, Japan) and analyzed using Panorama Fluorescence v. 2.1 software. Fluorescence emission spectra ranging from 360 to 450 nm of the sample solutions were recorded using an excitation wavelength of 334 nm at room temperature. Each measurement was repeated in triplicate.

Inductively coupled plasma-mass spectrometry (ICP-MS) was performed on a PerkinElmer SCIEX ICP mass spectrometer ELAN DRC II, equipped with high-speed quadrupole, dynamic reaction cell (DRC) and axial field technology (AFT) to completely eliminate polyatomic interferences, using 1%  $\text{HNO}_3$  as the matrix and rhodium (Rh) as the internal standard.

Analysis of lactic acid by the colorimetric assay was made on a SpectraMax M5 microplate reader.

**Synthesis of Monomer, 2-(But-3-yn-1-yloxy)-2-oxo-1,3,2-dioxaphospholane (BYP).** A solution of COP (14.9936 g, 105 mmol) in 50 mL of anhydrous THF was added dropwise to a stirred solution of 3-butyne-1-ol (8.1270 g, 116 mmol) and TEA (17 mL, 12 g, 120 mmol) in 200 mL of anhydrous THF at 4 °C. The reaction mixture was allowed to stir for 11 h at 4 °C and then for 30 min at room temperature. The precipitate was filtered off, and the filtrate was concentrated under reduced pressure. The filtrate was distilled under reduced pressure to obtain a faint yellow and viscous liquid (110–120 °C, 0.5 mmHg) with a yield of 52.3%, 9.67 g, IR: 3330–3170, 3050–2870, 1474, 1283, 1009, 926, 835, 756  $\text{cm}^{-1}$ .  $^1\text{H}$  NMR ( $\text{CDCl}_3$ , ppm):  $\delta$  4.50–4.31 (m, 4H,  $\text{POCH}_2\text{CH}_2\text{OP}$ ), 4.21 (dt,  $J = 9.3$  Hz,  $J = 6.9$  Hz, 2H,  $\text{POCH}_2\text{CH}_2\text{C}$ ), 2.59 (ddt,  $J = 6.9$  Hz, 2.4 Hz, 3H, 2H,  $\text{POCH}_2\text{CH}_2\text{C}$ ), 2.02 (t,  $J = 2.7$  Hz, 1H,  $\text{POCH}_2\text{CH}_2\text{CCH}$ ).  $^{13}\text{C}$  NMR ( $\text{CDCl}_3$ , ppm):  $\delta$  79.21, 70.58, 66.34 (d,  $J = 23.7$  Hz), 66.14 (d,  $J = 10.2$  Hz), 20.82 (d,  $J = 25.5$  Hz).  $^{31}\text{P}$  NMR ( $\text{CDCl}_3$ , ppm):  $\delta$  18.02. +ESI MS: calculated [M + H]<sup>+</sup> for  $\text{C}_6\text{H}_9\text{O}_4\text{P}$ , 177.0317; found, 177.0311.

**Synthesis of Diblock Copolymer, Poly(butynyl phosphotriester)<sub>50</sub>-block-Poly(*l*-lactide)<sub>50</sub> (PE<sub>50</sub>-*b*-PLLA<sub>50</sub>).** In a glovebox, a solution of BYP

(3.0226 g, 17.2 mmol) and benzyl alcohol (35.3  $\mu$ L, 37.0 mg, 0.340 mmol) in anhydrous DCM (3.0 mL) was transferred into a vial with a stir bar. DBU (102  $\mu$ L, 104 mg, 0.682 mmol) was added via pipet into the mixture solution. After the mixture stirred for 7 min, a solution of LLA (2.4615 g, 17.1 mmol) in anhydrous DCM (21 mL) was quickly added into the mixture solution. After 4 min, the reaction was quenched by addition of a solution of benzoic acid in DCM (excess). The product was precipitated in diethyl ether (3 $\times$ ) and dried overnight under vacuum to afford the diblock copolymer product as a tacky white solid (4.9787 g, 91% yield). GPC:  $M_n = 21\,800$  g/mol, PDI = 1.17. IR: 3350–3150, 3050–2850, 1757, 1456, 1271, 1211, 1184, 1130, 1074, 1009, 970, 804  $\text{cm}^{-1}$ .  $^1\text{H}$  NMR ( $\text{CD}_2\text{Cl}_2$ , ppm):  $\delta$  7.44–7.32 (m, 5H, aromatic ring), 5.16 (broad q,  $J = 7.2$  Hz, 102H,  $\text{ArCH}_2\text{OP}$  and  $\text{OCCH}(\text{O})\text{CH}_3$ ), 4.40–4.22 (b, 200H,  $\text{POCH}_2\text{CH}_2\text{O}$ ), 4.22–4.08 (b, 100H,  $\text{POCH}_2\text{CH}_2\text{CCH}$ ), 2.67–2.54 (b, 100H,  $\text{POCH}_2\text{CH}_2\text{CCH}$ ), 2.28–2.09 (b, 50H,  $\text{OCH}_2\text{CH}_2\text{CCH}$ ), 1.55 (broad d,  $J = 7.2$  Hz, 300H,  $\text{CH}_3\text{CH}(\text{O})\text{CO}$ ).  $^{13}\text{C}$  NMR ( $\text{CD}_2\text{Cl}_2$ , ppm):  $\delta$  170.02, 130.07, 129.16, 128.57, 80.28, 71.00, 69.52, 67.00, 66.26, 21.06, 17.02.  $^{31}\text{P}$  NMR ( $\text{CD}_2\text{Cl}_2$ , ppm):  $\delta$  –1.02. DSC:  $T_g = -33$   $^\circ\text{C}$ . TGA in  $\text{N}_2$ : 190–290  $^\circ\text{C}$ , 40% mass loss; 290–370  $^\circ\text{C}$ , 42% mass loss; 12% mass remaining above 370  $^\circ\text{C}$ .

**Synthesis of Diblock Copolymer, Poly(butynyl phosphotriester)<sub>90</sub>-block-Poly(l-lactide)<sub>50</sub> (PPE<sub>90</sub>-b-PLLA<sub>50</sub>).** In a glovebox, a solution of BYP (2.0014 g, 11.4 mmol) and benzyl alcohol (11.8  $\mu$ L, 12.3 mg, 0.114 mmol) in anhydrous DCM (2.0 mL) was transferred into a vial with a stir bar. DBU (34  $\mu$ L, 34.6 mg, 0.228 mmol) was added via pipet into the mixture solution. After the mixture stirred for 8 min, a solution of LLA (1.6434 g, 11.4 mmol) in anhydrous DCM (14.2 mL) was quickly added via pipet into the reaction mixture. After 4.5 min, the reaction was quenched by addition of a solution of benzoic acid in DCM (excess). The product was precipitated in diethyl ether (3 $\times$ ) and dried overnight under vacuum to afford the diblock copolymer product as a tacky white solid (2.0574 g, 78% yield). GPC:  $M_n = 22\,400$  g/mol, PDI = 1.25. IR: 3350–3150, 3050–2850, 1757, 1454, 1383, 1360, 1271, 1211, 1186, 1130, 1072, 1011, 970, 860, 802, 752  $\text{cm}^{-1}$ .  $^1\text{H}$  NMR ( $\text{CD}_2\text{Cl}_2$ , ppm):  $\delta$  7.44–7.32 (m, 5H, aromatic ring), 5.17 (broad q,  $J = 7.2$  Hz, 102H,  $\text{ArCH}_2\text{OP}$  and  $\text{OCCH}(\text{O})\text{CH}_3$ ), 4.38–4.22 (b, 360H,  $\text{POCH}_2\text{CH}_2\text{O}$ ), 4.22–4.10 (b, 180H,  $\text{POCH}_2\text{CH}_2\text{CCH}$ ), 2.68–2.53 (b, 180H,  $\text{POCH}_2\text{CH}_2\text{CCH}$ ), 2.24–2.07 (b, 90H,  $\text{OCH}_2\text{CH}_2\text{CCH}$ ), 1.56 (broad d,  $J = 7.2$  Hz, 300H,  $\text{CH}_3\text{CH}(\text{O})\text{CO}$ ).  $^{13}\text{C}$  NMR ( $\text{CD}_2\text{Cl}_2$ , ppm):  $\delta$  170.02, 129.16, 128.57, 80.28, 71.00, 69.52, 67.00, 66.26, 21.06, 17.02.  $^{31}\text{P}$  NMR ( $\text{CD}_2\text{Cl}_2$ , ppm):  $\delta$  –1.02. DSC:  $T_g = -29$   $^\circ\text{C}$ . TGA in  $\text{N}_2$ : 275  $^\circ\text{C}$ , 35% mass loss; 350  $^\circ\text{C}$ , 32% mass loss; 32% mass remaining above 350  $^\circ\text{C}$ .

**Synthesis of Diblock Copolymer, Poly(butynyl phosphotriester)<sub>210</sub>-block-Poly(l-lactide)<sub>50</sub> (PPE<sub>210</sub>-b-PLLA<sub>50</sub>).** In a glovebox, a solution of BYP (1.9973 g, 11.3 mmol) and benzyl alcohol (3.9  $\mu$ L, 4.1 mg, 0.038 mmol) in anhydrous DCM (2.3 mL) was transferred into a vial with a stir bar. DBU (17  $\mu$ L, 17 mg, 0.11 mmol) was added via pipet into the reaction mixture. After the mixture stirred for 30 min, a solution of LLA (0.5451 g, 3.78 mmol) in anhydrous DCM (3.4106 mL) was quickly added via pipet into the reaction mixture. After 4.5 min, the reaction was quenched by addition of a solution of benzoic acid in DCM (excess). The product was precipitated in diethyl ether (3 $\times$ ) and dried overnight under vacuum to afford the diblock copolymer product as a tacky white solid (1.3689 g, 82% yield). GPC:  $M_n = 45\,600$  g/mol, PDI = 1.26. IR: 3325–3125, 3025–2825, 1757, 1454, 1383, 1267, 1188, 1128, 1072, 1009, 972, 847, 804, 735  $\text{cm}^{-1}$ .  $^1\text{H}$  NMR ( $\text{CD}_2\text{Cl}_2$ , ppm):  $\delta$  7.44–7.32 (m, 5H, aromatic ring), 5.16 (broad q,  $J = 7.2$  Hz, 102H,  $\text{ArCH}_2\text{OP}$  and  $\text{OCCH}(\text{O})\text{CH}_3$ ), 4.38–4.22 (b, 840H,  $\text{POCH}_2\text{CH}_2\text{O}$ ), 4.22–4.10 (b, 420H,  $\text{POCH}_2\text{CH}_2\text{CCH}$ ), 2.68–2.53 (b, 420H,  $\text{POCH}_2\text{CH}_2\text{CCH}$ ), 2.24–2.07 (b, 210H,  $\text{OCH}_2\text{CH}_2\text{CCH}$ ), 1.56 (broad d,  $J = 7.2$  Hz, 300H,  $\text{CH}_3\text{CH}(\text{O})\text{CO}$ ).  $^{13}\text{C}$  NMR ( $\text{CD}_2\text{Cl}_2$ , ppm):  $\delta$  170.02, 129.15, 128.57, 80.27, 70.99, 69.52, 67.01, 66.26, 21.05, 17.01.  $^{31}\text{P}$  NMR ( $\text{CD}_2\text{Cl}_2$ , ppm):  $\delta$  –1.03. DSC:  $T_g = -42$   $^\circ\text{C}$ . TGA in  $\text{N}_2$ : 275  $^\circ\text{C}$ , 45% mass loss; 360  $^\circ\text{C}$ , 20% mass loss; 360  $^\circ\text{C}$ , 35% mass remaining above 360  $^\circ\text{C}$ .

**Thiol-yne "Click" Reaction of Alkyne Side Chain Moieties of PPE Block of PPE<sub>50</sub>-b-PLLA<sub>50</sub> with 3-Mercaptopropionic Acid, 2a.** A solution of PPE<sub>50</sub>-b-PLLA<sub>50</sub> (0.1493 g, 0.00990 mmol), 3-mercaptopropionic acid (0.430 mL, 4.93 mmol), and 2,2-dimethoxy-2-phenylacetophenone (0.2153 g, 0.840 mmol) in 7.5 mL of DMSO was irradiated

under UV irradiation (365 nm, 6 W) for 60 min while stirring. Purification included precipitation in diethyl ether (3 $\times$ ), followed by dialysis in nanopure water, and isolation of the product by freeze-drying overnight to give a tacky white solid (0.1892 mg, 75% yield). IR: 3675–2760, 2700–2430, 1757, 1715, 1452, 1408, 1385, 1184, 1130, 1086, 1016, 982, 802, 754  $\text{cm}^{-1}$ .  $^1\text{H}$  NMR (DMSO- $d_6$ , ppm):  $\delta$  13.2–11.9 (b,  $\text{SCH}_2\text{CH}_2\text{C(O)OH}$ ), 7.44–7.26 (m, 5H, aromatic ring), 5.46 (d,  $J = 7.2$  Hz, 2H,  $\text{ArCH}_2\text{O}$ ), 5.20 (broad q,  $J = 7.2$  Hz, 100H,  $\text{OCCH}(\text{O})\text{CH}_3$ ), 4.50–3.80 (b, 300H,  $\text{POCH}_2\text{CH}_2\text{O}$  and  $\text{POCH}_2\text{CH}_2\text{CH}$ ), 3.00–2.81 (b, 200H,  $\text{SCH}_2\text{CH}_2\text{COOH}$ ), 2.80–2.62 (b, 250H,  $\text{SCH}_2\text{CH}_2\text{COOH}$  and  $\text{SCH}(\text{CH}_2)\text{CH}_2\text{CH}_2\text{O}$ ), 2.60–2.50 (b, 100H,  $\text{SCH}_2\text{CHS}$ ), 2.25–2.05 and 1.85–1.57 (b, 100H,  $\text{POCH}_2\text{CH}_2\text{CH}$ ), 1.46 (broad d,  $J = 7.2$  Hz, 300H,  $\text{OCCH}(\text{O})\text{CH}_3$ ).  $^{13}\text{C}$  NMR (DMSO, ppm):  $\delta$  173.05, 172.19, 169.27, 68.72, 66.25, 65.34, 44.05, 42.91, 41.67, 38.19, 37.54, 34.73, 34.18, 33.53, 29.71, 27.18, 26.09, 25.22, 16.53.  $^{31}\text{P}$  NMR (DMSO, ppm):  $\delta$  –0.03. DSC:  $T_g = 6$   $^\circ\text{C}$ . TGA in  $\text{N}_2$ : 105–190  $^\circ\text{C}$ , 13% mass loss; 190–280  $^\circ\text{C}$ , 40% mass loss; 280–350  $^\circ\text{C}$ , 25% mass loss; 22% mass remaining above 350  $^\circ\text{C}$ .

**Thiol-yne "Click" Reaction of Alkyne Side Chain Moieties of PPE Block of PPE<sub>90</sub>-b-PLLA<sub>50</sub> with 3-Mercaptopropionic Acid, 2b.** A solution of PPE<sub>90</sub>-b-PLLA<sub>50</sub> (0.1014 mg, 0.00437 mmol), 3-mercaptopropionic acid (0.34 mL, 3.90 mmol), and 2,2-dimethoxy-2-phenylacetophenone (0.1975 g, 0.771 mmol) in 7.5 mL of DMSO was irradiated under UV irradiation (365 nm, 6 W) for 60 min while stirring. Purification included precipitation in diethyl ether (3 $\times$ ), followed by dialysis in nanopure water, and isolation of the product by freeze-drying overnight to give a tacky white solid (0.1512 mg, 82% yield). IR: 3375–2775, 2715–2400, 1713, 1404, 1180, 1130, 1074, 1020, 955, 799  $\text{cm}^{-1}$ .  $^1\text{H}$  NMR (DMSO, ppm):  $\delta$  13.2–12.2 (b,  $\text{SCH}_2\text{CH}_2\text{C(O)OH}$ ), 7.45–7.30 (m, 5H, aromatic ring), 5.20 (broad q,  $J = 7.2$  Hz, 100H,  $\text{OCCH}(\text{O})\text{CH}_3$ ), 4.35–3.70 (b, 540H,  $\text{POCH}_2\text{CH}_2\text{O}$  and  $\text{POCH}_2\text{CH}_2\text{CH}$ ), 3.00–2.80 (b, 360H,  $\text{SCH}_2\text{CH}_2\text{COOH}$ ), 2.80–2.64 (b, 450H,  $\text{SCH}_2\text{CH}_2\text{COOH}$  and  $\text{SCH}(\text{CH}_2)\text{CH}_2\text{CH}_2\text{O}$ ), 2.58–2.42 (b, 180H,  $\text{SCH}_2\text{CHS}$ ), 2.25–2.05 and 1.85–1.60 (b, 180H,  $\text{POCH}_2\text{CH}_2\text{CH}$ ), 1.46 (broad d,  $J = 7.2$  Hz, 300H,  $\text{OCCH}(\text{O})\text{CH}_3$ ).  $^{13}\text{C}$  NMR (DMSO, ppm):  $\delta$  172.86, 172.13, 169.21, 68.68, 64.56, 47.13, 46.80, 44.02, 42.92, 36.79, 34.82, 34.16, 29.27, 26.14, 16.49.  $^{31}\text{P}$  NMR (DMSO, ppm):  $\delta$  –0.02. DSC:  $T_g = 5$   $^\circ\text{C}$ . TGA in  $\text{N}_2$ : 250  $^\circ\text{C}$ , 48% mass loss; 365  $^\circ\text{C}$ , 28% mass loss; 24% mass remaining above 365  $^\circ\text{C}$ .

**Thiol-yne "Click" Reaction of Alkyne Side Chain Moieties of PPE Block of PPE<sub>210</sub>-b-PLLA<sub>50</sub> with 3-Mercaptopropionic Acid, 2c.** A solution of PPE<sub>210</sub>-b-PLLA<sub>50</sub> (0.1983 mg, 0.00448 mmol), 3-mercaptopropionic acid (0.83 g, 9.52 mmol), and 2,2-dimethoxy-2-phenylacetophenone (0.4769 g, 1.86 mmol) in 9 mL of DMSO was irradiated under UV irradiation (365 nm, 6 W) for 60 min while stirring. Purification included precipitation in diethyl ether (3 $\times$ ), followed by dialysis in nanopure water, and isolation of the product by freeze-drying overnight to give a tacky white solid (0.3452 g, 86.0% yield). IR: 3675–2775, 2775–2350, 1713, 1404, 1182, 1130, 1020, 974, 953, 799  $\text{cm}^{-1}$ .  $^1\text{H}$  NMR (DMSO, ppm):  $\delta$  13.6–12.2 (b,  $\text{SCH}_2\text{CH}_2\text{C(O)OH}$ ), 7.45–7.30 (m, 5H, aromatic ring), 5.20 (broad q,  $J = 7.2$  Hz, 100H,  $\text{OCCH}(\text{O})\text{CH}_3$ ), 4.30–3.65 (b, 1260H,  $\text{POCH}_2\text{CH}_2\text{O}$  and  $\text{POCH}_2\text{CH}_2\text{CH}$ ), 3.00–2.78 (b, 840H,  $\text{SCH}_2\text{CH}_2\text{COOH}$ ), 2.78–2.65 (b, 1050H,  $\text{SCH}_2\text{CH}_2\text{COOH}$  and  $\text{SCH}(\text{CH}_2)\text{CH}_2\text{CH}_2\text{O}$ ), 2.60–2.40 (b, 420H,  $\text{SCH}_2\text{CH}_2\text{CH}_2\text{O}$ ), 2.30–2.08 and 1.85–1.55 (b, 420H,  $\text{POCH}_2\text{CH}_2\text{CH}$ ), 1.46 (broad d,  $J = 6.9$  Hz, 300H,  $\text{OCCH}(\text{O})\text{CH}_3$ ).  $^{13}\text{C}$  NMR (DMSO, ppm):  $\delta$  172.87, 172.16, 169.21, 164.52, 68.68, 47.19, 46.80, 44.02, 42.96, 36.85, 34.91, 34.17, 29.28, 26.29, 16.48.  $^{31}\text{P}$  NMR (DMSO, ppm):  $\delta$  –0.02. DSC:  $T_g = -10$   $^\circ\text{C}$ . TGA in  $\text{N}_2$ : 260  $^\circ\text{C}$ , 53% mass loss; 350  $^\circ\text{C}$ , 14% mass loss; 33% mass remaining above 350  $^\circ\text{C}$ .

**General Procedure for Self-Assembly of Amphiphilic Diblock Copolymers, Anionic Polyphosphoester-*b*-Poly(l-lactide) (aPPE-*b*-PLLA), 2.** A total of 1.0 mg of **2** was suspended in nanopure water (for TEM and AFM analyses), MOPS buffer (50 mM, pH 7.4), or ammonium acetate buffer (50 mM, pH 5.0) (for DLS and  $\zeta$ -potential measurements) in a vial, and the mixture stirred for 30 min at room temperature prior to sample preparation.

**Determination of Critical Micelle Concentrations (CMCs) for 2 To Afford Micelles 3 in Nanopure Water.** The CMCS for **2a**, **2b**, or **2c** in nanopure water were determined using pyrene as the fluorescent probe following the protocol in literature.<sup>55</sup> A total volume of 0.75 mL of sample solution was prepared by mixing **2** in

nanopure water (ranging from *ca.* 0.01–3.5 mg/mL) with a pyrene aqueous stock solution (0.250 mL,  $6.0 \times 10^{-7}$  mol/L). All the sample solutions were then stored at room temperature for 1 h followed by storage at 4 °C overnight to equilibrate the pyrene and the micelles. The fluorescence measurement was conducted at room temperature, in which the pyrene was excited at 334 nm and its emission spectrum was recorded at 373 and 384 nm, corresponding to the first and third vibrational peaks, respectively. All measurements were repeated in triplicate and the ratios of intensities of the first ( $I_1$ ) and third ( $I_{334}$ ) peaks were plotted against the concentrations of **3** in the sample solutions. The CMC was taken as the intersection of the tangent to the curve at the inflection with tangent through the points at lower polymer concentration.

**General Procedure for the Preparation of AgOAc-Loaded Degradable Polymeric Nanoparticles (AgOAc-3).** A solution of AgOAc (4 mg/mL in nanopure water) was added dropwise to a solution of **2** (1.5 mL, polymer concentration = 5 mg/mL). The solution was shielded from light and allowed to stir overnight at room temperature. Then, the solution was washed thoroughly with nanopure water (>4 cycles) to remove free small silver-compounds by using a centrifugal filter device (100 kDa MWCO). The absence of free Ag<sup>+</sup> from the mixture solution was confirmed by observing no occurrence of precipitates (AgCl) upon adding a saturated solution of sodium chloride to the filtrate. The resulting solution of AgOAc-**3** was reconstituted to a final volume of 2 mL, and silver concentration was measured by ICP-MS. Aliquots of the solution of AgOAc-**3** were used for UV-vis, TEM and DLS measurements.

**General Procedure for the Preparation of SCC22-Loaded Degradable Polymeric Nanoparticles (SCC22-3).** A solution of SCC22 (10 mg/mL in nanopure water) was added dropwise to the solution of **2** (1.5 mL, polymer concentration = 5 mg/mL). The solution was shielded from light and allowed to stir overnight at room temperature. Then, the solution was washed thoroughly with nanopure water (>4 cycles) to remove free small silver-compounds by using a centrifugal filter device (100 kDa MWCO). The absence of free Ag<sup>+</sup> from the mixture solution was confirmed by observing no occurrence of precipitates (AgCl) upon adding a saturated solution of sodium chloride to the filtrate. The resulting solution of SCC22-**3** was reconstituted to a final volume of 2 mL, and silver concentration was measured by ICP-MS. Aliquots of the solution of SCC22-**3** were used for UV-vis, TEM and DLS measurements.

**General Procedure for the Preparation of SCC10-Loaded Degradable Polymeric Nanoparticles (SCC10-3).** A solution of SCC10 (10 mg/mL in CHCl<sub>3</sub>) was added dropwise to a solution of **2** (1.5 mL, polymer concentration = 5 mg/mL). The solution was shielded from light and allowed to stir vigorously to form a water/CHCl<sub>3</sub> emulsion overnight at room temperature. After evaporation of the organic solvent overnight, the solution was washed thoroughly with nanopure water (>4 cycles) to remove free small silver-compounds by using a centrifugal filter device (100 kDa MWCO). The absence of free Ag<sup>+</sup> from the mixture solution was confirmed by observing no occurrence of precipitates (AgCl) upon adding a saturated solution of sodium chloride into the filtrate. The resulting solution of SCC10-**3** was reconstituted to a final volume of 2 mL, and silver concentration was measured by ICP-MS. Aliquots of the solution of SCC10-**3** were used for UV-vis, TEM and DLS measurements.

**General Procedure for Study of Silver Release Kinetics of Silver Compounds (AgOAc, SCC22, or SCC10) and Ag-3 (Loaded by AgOAc, SCC22, or SCC10).** Into a presoaked dialysis cassette (Slide-A-Lyzer, 10 kDa MWCO, Pierce Biotechnology, Rockford, IL) was transferred a solution of silver compounds or Ag-3 (3 mL). The dialysis cassette was incubated in nanopure water at 37 °C for 5 days. For SCC10, it was dissolved in THF, and the solution was transferred into the dialysis cassette. Aliquots (*ca.* 0.1 mL) of solution were extracted at predetermined intervals, and the concentration of silver was measured by ICP-MS. The final results were obtained from triplicate experiments.

**Investigation of Nanoparticle Stability in Aqueous Solution by Monitoring the Changes in Hydrodynamic Diameters of 3b, as Measured by DLS.** **2b** was dissolved (0.5 mg/mL) in MOPS buffer (50 mM, pH 7.4) or ammonium acetate buffer (50 mM, pH 5.0) in a vial. The

prepared solution was incubated in a shaker at 37 °C, and hydrodynamic diameter and  $\zeta$ -potential were monitored by using DLS and  $\zeta$ -potential, respectively, over time.

**Preparation and Identification of the Degradation Products of 3b.** A solution of **2b** (9.2 mg) in 2 mL of nanopure water was incubated in a shaker at 37 °C until the micelles were not detectable by DLS. The solution was lyophilized into a powder, and then analyzed by ESI MS, MALDI-TOF MS, and <sup>31</sup>P NMR spectroscopy.

**Study of Enzymatic Degradation of PLLA Block Segment of 3b Using Proteinase K (PK) and Porcine Liver Esterase (PLE).** The enzymatic degradation experiments was performed following our previous report.<sup>52</sup> A solution of **2b** (0.5 mL, 0.0032 mM, 0.32 mM of LLA) in 0.1 M Tris-HCl buffer at pH 7.4, containing 0.05% (w/v) NaN<sub>3</sub>, was placed in 1.5 mL centrifugation tubes. Two stock solutions of PLE and PK were also prepared in 0.1 M Tris-HCl buffer at pH 7.4, containing 0.05% (w/v) NaN<sub>3</sub>, to maintain similar enzymatic activities (*ca.* 1 U/ $\mu$ L). The solution of PLE (91  $\mu$ L, 5,482 U/mL) was diluted in 409  $\mu$ L of Tris-HCl buffer and the solution of PK (367  $\mu$ L, 1362 U/mL) was diluted in 133  $\mu$ L of Tris-HCl buffer. For the enzyme-catalyzed hydrolysis of nanoparticles, stock solutions of enzyme (50  $\mu$ L, 1 U/ $\mu$ L) were added to each tube, mixed by the use of a vortex, and incubated at 37 °C, using an incubating shaker. As a control, to determine the hydrolytic degradation rates of the PLLA block segment of the samples in the absence of enzyme catalysis, 50  $\mu$ L of Tris-HCl buffer was added to each solution (to maintain identical polymer concentrations as the enzyme catalyzed experiment) and incubated at 37 °C in a shaker. The lactate assays were performed following the standard protocol of ab65331 as described below. At time points 0, 1, 6, 12, and 24 h, 50  $\mu$ L of sample was withdrawn from each tube, mixed with 50  $\mu$ L of lactate enzyme assay mix in a 100  $\mu$ L Falcon clear well, protected from light and incubated at room temperature for 30 min to produce color, and analyzed using a plate reader for absorption at 450 nm. Each analysis was performed in triplicate, and average absorbance values with standard deviations were reported. A calibration curve of L-lactic acid was constructed by the use of serial dilutions that were produced from a standard solution of 0.1 M L-lactic acid in 0.1 M Tris-HCl buffer (calibration range: 0–10 nmol of lactate), and the production of L-lactic acid at each time point was quantified and reported as a percentage of the total theoretical L-lactic acid present in each solution at the predetermined concentrations.

**Antibacterial Activity.** Minimum inhibitory concentration (MIC) was determined by microdilution in Mueller-Hinton (MH) broth. Briefly, strains were streaked from glycerol stocks onto tryptic soy agar plates and grown overnight at 37 °C. In the following morning, colonies were suspended in MH media until OD<sub>650 nm</sub> = 0.2, and then incubated with shaking at 37 °C until OD<sub>650 nm</sub> = 0.4 ( $\sim 5 \times 10^8$  colony-forming units [CFU]/mL). Bacterial strains were then diluted to  $2 \times 10^5$  CFU/mL in MH media and finally diluted 1:1 with compounds.

Silver-compounds were resuspended fresh on the day of the experiment in sterile water to a working concentration of 200  $\mu$ g/mL silver. Each compound was then diluted in MH media to a dose between 0.5 and 12  $\mu$ g/mL and diluted 1:1 with bacteria. Plates were incubated statically overnight at 37 °C in the dark and read visually on the next day. The MIC was recorded as the lowest silver dose that did not permit bacterial growth.

Each compound was tested in duplicate or triplicate wells of a 96-well plate and repeated on 3–6 separate days. Results included 1–2 separate batches of compounds for a total of 9–15 trials of each compound with each bacterial strain. Naked **3**, *i.e.* **3** without silver-loading, was also examined, and the samples did not display any inhibitory activity within the ranges tested.

**Conflict of Interest:** The authors declare no competing financial interest.

**Supporting Information Available:** Additional characterization data. This material is available free of charge via the Internet at <http://pubs.acs.org>.

**Acknowledgment.** We gratefully acknowledge financial support from the National Heart Lung and Blood Institute as a

Program of Excellence in Nanotechnology (HHSN268201000046C) and from the National Institute of Diabetes and Digestive and Kidney Diseases (R01-DK082546). The Welch Foundation is gratefully acknowledged for support through the W. T. Doherty-Welch Chair in Chemistry, Grant No. A-0001. The transmission electron microscopy facilities and Dr. Hansoo Kim at the Microscopy & Imaging Center at Texas A&M University are gratefully acknowledged. We also thank Dr. Stephanie Fritz for collection of the *S. aureus* isolates.

## REFERENCES AND NOTES

- Huh, A. J.; Kwon, Y. J. "Nanoantibiotics": A New Paradigm for Treating Infectious Diseases Using Nanomaterials in the Antibiotics Resistant Era. *J. Controlled Release* **2011**, *156*, 128–145.
- Koul, A.; Arnoult, E.; Lounis, N.; Guillemont, J.; Andries, K. The Challenge of New Drug Discovery for Tuberculosis. *Nature* **2011**, *469*, 483–490.
- Allen, T.; Cullis, P. Drug Delivery Systems: Entering the Mainstream. *Science* **2004**, *303*, 1818–1822.
- Taubes, G. The Bacteria Fight Back. *Science* **2008**, *321*, 356–361.
- Mitragotri, S.; Burke, P. A.; Langer, R. Overcoming the Challenges in Administering Biopharmaceuticals: Formulation and Delivery Strategies. *Nat. Rev. Drug Discovery* **2014**, *13*, 655–672.
- Zhang, L.; Gu, F. X.; Chan, J. M.; Wang, A. Z.; Langer, R. S.; Farokhzad, O. C. Nanoparticles in Medicine: Therapeutic Applications and Developments. *Clin. Pharmacol. Ther.* **2008**, *83*, 761–769.
- Rizzello, L.; Pompa, P. P. Nanosilver-Based Antibacterial Drugs and Devices: Mechanisms, Methodological Drawbacks, and Guidelines. *Chem. Soc. Rev.* **2014**, *43*, 1501–1518.
- Melaiye, A.; Youngs, W. J. Silver and Its Application as an Antimicrobial Agent. *Expert Opin. Ther. Pat.* **2005**, *15*, 125–130.
- Silver, S. Bacterial Silver Resistance: Molecular Biology and Uses and Misuses of Silver Compounds. *FEMS Microbiol. Rev.* **2003**, *27*, 341–353.
- Gupta, A.; Matsui, K.; Lo, J.-F.; Silver, S. Molecular Basis for Resistance to Silver Cations in *Salmonella*. *Nat. Med.* **1999**, *5*, 183–188.
- Lansdown, A. B. Silver. I: Its Antibacterial Properties and Mechanism of Action. *J. Wound Care* **2002**, *11*, 125–130.
- Mijnendonckx, K.; Leyss, N.; Mahillon, J.; Silver, S.; Van Houdt, R. Antimicrobial Silver: Uses, Toxicity and Potential for Resistance. *BioMetals* **2013**, *26*, 609–621.
- Balogh, L.; Swanson, D. R.; Tomalia, D. A.; Hagnauer, G. L.; McManus, A. T. Dendrimer–Silver Complexes and Nanocomposites as Antimicrobial Agents. *Nano Lett.* **2001**, *1*, 18–21.
- Sambhy, V.; MacBride, M. M.; Peterson, B. R.; Sen, A. Silver Bromide Nanoparticle/Polymer Composites: Dual Action Tunable Antimicrobial Materials. *J. Am. Chem. Soc.* **2006**, *128*, 9798–9808.
- Aymonier, C.; Schlotterbeck, U.; Antonietti, L.; Zacharias, P.; Thomann, R.; Tiller, J. C.; Mecking, S. Hybrids of Silver Nanoparticles with Amphiphilic Hyperbranched Macromolecules Exhibiting Antimicrobial Properties. *Chem. Commun.* **2002**, *8*, 3018–3019.
- Cannon, C. L.; Hogue, L. A.; Vajravelu, R. K.; Capps, G. H.; Ibricevic, A.; Hindi, K. M.; Kascatan-Nebioglu, A.; Walter, M. J.; Brody, S. L.; Youngs, W. J. *In Vitro* and Murine Efficacy and Toxicity Studies of Nebulized SCC1, a Methylated Caffeine-Silver(I) Complex, for Treatment of Pulmonary Infections. *Antimicrob. Agents Chemother.* **2009**, *53*, 3285–3293.
- Garrison, J. C.; Youngs, W. J. Ag(I) N-Heterocyclic Carbene Complexes: Synthesis, Structure, and Application. *Chem. Rev.* **2005**, *105*, 3978–4008.
- Hindi, K.; Siciliano, T.; Durmus, S.; Panzner, M.; Medvetz, D.; Reddy, D. V.; Hogue, L.; Hovis, C.; Hilliard, J.; Mallet, R.; et al. Synthesis, Stability, and Antimicrobial Studies of Electronically Tuned Silver Acetate N-Heterocyclic Carbene. *J. Med. Chem.* **2008**, *51*, 1577–1583.
- Kascatan Nebioglu, A.; Melaiye, A.; Hindi, K.; Durmus, S.; Panzner, M.; Hogue, L.; Mallett, R.; Hovis, C.; Coughenour, M.; Crosby, S.; et al. Synthesis from Caffeine of a Mixed N-Heterocyclic Carbene–Silver Acetate Complex Active against Resistant Respiratory Pathogens. *J. Med. Chem.* **2006**, *49*, 6811–6818.
- Kascatan Nebioglu, A.; Panzner, M.; Tessier, C.; Cannon, C.; Youngs, W. N-Heterocyclic Carbene–Silver Complexes: A New Class of Antibiotics. *Coord. Chem. Rev.* **2007**, *251*, 884–895.
- Youngs, W. J.; Knapp, A. R.; Wagers, P. O.; Tessier, C. A. Nanoparticle Encapsulated Silver Carbene Complexes and Their Antimicrobial and Anticancer Properties: A Perspective. *Dalton Trans.* **2012**, *41*, 327–336.
- Leid, J. G.; Ditto, A. J.; Knapp, A.; Shah, P. N.; Wright, B. D.; Blust, R.; Christensen, L.; Clemons, C. B.; Wilber, J. P.; Young, G. W.; et al. *In Vitro* Antimicrobial Studies of Silver Carbene Complexes: Activity of Free and Nanoparticle Carbene Formulations against Clinical Isolates of Pathogenic Bacteria. *J. Antimicrob. Chemother.* **2012**, *67*, 138–148.
- Hindi, K. M.; Panzner, M. J.; Tessier, C. A.; Cannon, C. L.; Youngs, W. J. The Medicinal Applications of Imidazolium Carbene–Metal Complexes. *Chem. Rev.* **2009**, *109*, 3859–3884.
- Panzner, M. J.; Hindi, K. M.; Wright, B. D.; Taylor, J. B.; Han, D. S.; Youngs, W. J.; Cannon, C. L. A Theobromine Derived Silver N-Heterocyclic Carbene: Synthesis, Characterization, and Antimicrobial Efficacy Studies on Cystic Fibrosis Relevant Pathogens. *Dalton Trans.* **2009**, *7308–7313*.
- Hindi, K. M.; Ditto, A. J.; Panzner, M. J.; Medvetz, D. A.; Han, D. S.; Hovis, C. E.; Hilliard, J. K.; Taylor, J. B.; Yun, Y. H.; Cannon, C. L.; et al. The Antimicrobial Efficacy of Sustained Release Silver–Carbene Complex–Loaded L-Tyrosine Polyphosphate Nanoparticles: Characterization, *In Vitro* and *In Vivo* Studies. *Biomaterials* **2009**, *30*, 3771–3779.
- Elsabahy, M.; Wooley, K. Design of Polymeric Nanoparticles for Biomedical Delivery Applications. *Chem. Soc. Rev.* **2012**, *41*, 2545–2561.
- Elsabahy, M.; Wooley, K. L. Strategies toward Well-Defined Polymer Nanoparticles Inspired by Nature: Chemistry versus Versatility. *J. Polym. Sci., Part A: Polym. Chem.* **2012**, *50*, 1869–1880.
- Li, Y.; Hindi, K.; Watts, K. M.; Taylor, J. B.; Zhang, K.; Li, Z.; Hunstad, D. A.; Cannon, C. L.; Youngs, W. J.; Wooley, K. L. Shell Crosslinked Nanoparticles Carrying Silver Antimicrobials as Therapeutics. *Chem. Commun.* **2010**, *46*, 121–123.
- Shah, P. N.; Lin, L. Y.; Smolen, J. A.; Tagaev, J. A.; Gunsten, S. P.; Han, D. S.; Heo, G. S.; Li, Y.; Zhang, F.; Zhang, S.; et al. Synthesis, Characterization, and *In Vivo* Efficacy of Shell Cross-Linked Nanoparticle Formulations Carrying Silver Antimicrobials as Aerosolized Therapeutics. *ACS Nano* **2013**, *7*, 4977–4987.
- Kumari, A.; Yadav, S. K.; Yadav, S. C. Biodegradable Polymeric Nanoparticles Based Drug Delivery Systems. *Colloids Surf., B* **2010**, *75*, 1–18.
- Zhao, Z.; Wang, J.; Mao, H.-Q.; Leong, K. W. Polyphosphoesters in Drug and Gene Delivery. *Adv. Drug Delivery Rev.* **2003**, *55*, 483–499.
- Tempelaar, S.; Mespouille, L.; Coulembier, O.; Dubois, P.; Dove, A. P. Synthesis and Post-Polymerisation Modifications of Aliphatic Poly(carbonate)s Prepared by Ring-Opening Polymerisation. *Chem. Soc. Rev.* **2013**, *42*, 1312–1336.
- Kamber, N. E.; Jeong, W.; Waymouth, R. M.; Pratt, R. C.; Lohmeijer, B. G. G.; Hedrick, J. L. Organocatalytic Ring-Opening Polymerization. *Chem. Rev.* **2007**, *107*, 5813–5840.
- Pounder, R. J.; Dove, A. P. Towards Poly(ester) Nanoparticles: Recent Advances in the Synthesis of Functional Poly(ester)s by Ring-Opening Polymerization. *Polym. Chem.* **2010**, *1*, 260–271.
- Hadjichristidis, N.; Iatrou, H.; Pitsikalis, M.; Sakellariou, G. Synthesis of Well-Defined Polypeptide-Based Materials

- via the Ring-Opening Polymerization of  $\alpha$ -Amino Acid N-Carboxyanhydrides. *Chem. Rev.* **2009**, *109*, 5528–5578.
36. Kricheldorf, H. R. Polypeptides and 100 Years of Chemistry of  $\alpha$ -Amino Acid N-Carboxyanhydrides. *Angew. Chem., Int. Ed.* **2006**, *45*, 5752–5784.
  37. Zhang, S.; Zou, J.; Zhang, F.; Elsabahy, M.; Felder, S. E.; Zhu, J.; Pochan, D. J.; Wooley, K. L. Rapid and Versatile Construction of Diverse and Functional Nanostructures Derived from a Polyphosphoester-Based Biomimetic Block Copolymer System. *J. Am. Chem. Soc.* **2012**, *134*, 18467–18474.
  38. Lim, Y. H.; Heo, G. S.; Cho, S.; Wooley, K. L. Construction of a Reactive Diblock Copolymer, Polyphosphoester-block-Poly(*L*-lactide), as a Versatile Framework for Functional Materials That Are Capable of Full Degradation and Nanoscopic Assembly Formation. *ACS Macro Lett.* **2013**, *2*, 785–789.
  39. Lim, Y. H.; Heo, G. S.; Rezenom, Y. H.; Pollack, S.; Raymond, J. E.; Elsabahy, M.; Wooley, K. L. Development of a Vinyl Ether-Functionalized Polyphosphoester as a Template for Multiple Postpolymerization Conjugation Chemistries and Study of Core Degradable Polymeric Nanoparticles. *Macromolecules* **2014**, *47*, 4634–4644.
  40. Gustafson, T. P.; Lim, Y. H.; Flores, J. A.; Heo, G. S.; Zhang, F.; Zhang, S.; Samarajeewa, S.; Raymond, J. E.; Wooley, K. L. Holistic Assessment of Covalently Labeled Core–Shell Polymeric Nanoparticles with Fluorescent Contrast Agents for Theranostic Applications. *Langmuir* **2014**, *30*, 631–641.
  41. Elsabahy, M.; Zhang, S.; Zhang, F.; Deng, Z. J.; Lim, Y. H.; Wang, H.; Parsamian, P.; Hammond, P. T.; Wooley, K. L. Surface Charges and Shell Crosslinks Each Play Significant Roles in Mediating Degradation, Biofouling, Cytotoxicity and Immunotoxicity for Polyphosphoester-Based Nanoparticles. *Sci. Rep.* **2013**, *3*, 3313.
  42. Gustafson, T. P.; Lonnecker, A. T.; Heo, G. S.; Zhang, S.; Dove, A. P.; Wooley, K. L. Poly(*D*-glucose carbonate) Block Copolymers: A Platform for Natural Product-Based Nanomaterials with Solvothermotic Characteristics. *Biomacromolecules* **2013**, *14*, 3346–3353.
  43. Fan, J.; Li, R.; He, X.; Seetho, K.; Zhang, F.; Zou, J.; Wooley, K. L. Construction of a Versatile and Functional Nanoparticle Platform Derived from a Helical Diblock Copolypeptide-Based Biomimetic Polymer. *Polym. Chem.* **2014**, *5*, 3977–3981.
  44. Aweda, T. A.; Zhang, S.; Mupanomunda, C.; Burkemper, J.; Heo, G. S.; Bandara, N.; Lin, M.; Cutler, C.; Cannon, C. L.; Youngs, W., et al. Investigating the Pharmacokinetics and Biological Distribution of Silver-Loaded Polyphosphoester-Based Nanoparticles Using  $^{111}\text{Ag}$  as a Radiotracer. *J. Pharm. Sci.*, submitted for publication.
  45. Garlotta, D. A Literature Review of Poly(lactic acid). *J. Polym. Environ.* **2001**, *9*, 63–84.
  46. Athanasiou, K. A.; Niederauer, G. G.; Agrawal, C. M. Sterilization, Toxicity, Biocompatibility and Clinical Applications of Polylactic Acid/Polyglycolic Acid Copolymers. *Biomaterials* **1996**, *17*, 93–102.
  47. Xiong, M.-H.; Bao, Y.; Yang, X.-Z.; Wang, Y.-C.; Sun, B.; Wang, J. Lipase-Sensitive Polymeric Triple-Layered Nanogel for “On-Demand” Drug Delivery. *J. Am. Chem. Soc.* **2012**, *134*, 4355–4362.
  48. Wang, D.-A.; Williams, C. G.; Yang, F.; Cher, N.; Lee, H.; Elisseeff, J. H. Bioresponsive Phosphoester Hydrogels for Bone Tissue Engineering. *Tissue Eng.* **2005**, *11*, 201–213.
  49. Baran, J.; Penczek, S. Hydrolysis of Polyesters of Phosphoric Acid. 1. Kinetics and the pH Profile. *Macromolecules* **1995**, *28*, 5167–5176.
  50. Wang, X.; Xie, X.; Cai, C.; Rytting, E.; Steele, T.; Kissel, T. Biodegradable Branched Polyesters Poly(vinyl sulfonate-covinyl alcohol)-graft Poly(*D,L*-lactic-coglycolic acid) as a Negatively Charged Polyelectrolyte Platform for Drug Delivery: Synthesis and Characterization. *Macromolecules* **2008**, *41*, 2791–2799.
  51. Iwasaki, Y.; Nakagawa, C.; Ohtomi, M.; Ishihara, K.; Akiyoshi, K. Novel Biodegradable Polyphosphate Cross-Linker for Making Biocompatible Hydrogel. *Biomacromolecules* **2004**, *5*, 1110–1115.
  52. Samarajeewa, S.; Zentay, R. P.; Jhurry, N. D.; Li, A.; Seetho, K.; Zou, J.; Wooley, K. L. Programmed Hydrolysis of Nanoassemblies by Electrostatic Interaction-Mediated Enzymatic-Degradation. *Chem. Commun.* **2014**, *50*, 968–970.
  53. Panzner, M. J.; Deeraksa, A.; Smith, A.; Wright, B. D.; Hindi, K. M.; Kascatan-Neboiglu, A.; Torres, A. G.; Judy, B. M.; Hovis, C. E.; Hilliard, J. K., et al. Synthesis and *in Vitro* Efficacy Studies of Silver Carbene Complexes on Biosafety Level 3 Bacteria. *Eur. J. Inorg. Chem.* **2009**, 1739–1745.
  54. Youngs, W. J.; Medvetz, D. A.; Hindi, K. M.; Panzner, M. J.; Ditto, A. J.; Yun, Y. H. Anticancer Activity of Ag(I) N-Heterocyclic Carbene Complexes Derived from 4,5-Dichloro-1*H*-imidazole. *Met.-Based Drugs* **2008**, *2008*, 1–7.
  55. Dominguez, A.; Fernandez, A.; Gonzalez, N.; Iglesias, E.; Montenegro, L. Determination of Critical Micelle Concentration of Some Surfactants by Three Techniques. *J. Chem. Educ.* **1997**, *74*, 1227–1231.